

3-10-1998

# Temperature Variations and N/O in the Orion Nebula from *HST* Observations

R. H. Rubin

*NASA/Ames Research Center*

P. G. Martin

*University of Toronto, Canada*

R. J. Dufour

*Rice University*

Gary J. Ferland

*University of Kentucky, gary@uky.edu*

J. A. Baldwin

*Cerro Tololo Inter-American Observatory, Chile*

*See next page for additional authors*

**Right click to open a feedback form in a new tab to let us know how this document benefits you.**

Follow this and additional works at: [https://uknowledge.uky.edu/physastron\\_facpub](https://uknowledge.uky.edu/physastron_facpub)

 Part of the [Astrophysics and Astronomy Commons](#), and the [Physics Commons](#)

## Repository Citation

Rubin, R. H.; Martin, P. G.; Dufour, R. J.; Ferland, Gary J.; Baldwin, J. A.; Hester, J. J.; and Walter, D. K., "Temperature Variations and N/O in the Orion Nebula from *HST* Observations" (1998). *Physics and Astronomy Faculty Publications*. 118.

[https://uknowledge.uky.edu/physastron\\_facpub/118](https://uknowledge.uky.edu/physastron_facpub/118)

This Article is brought to you for free and open access by the Physics and Astronomy at UKnowledge. It has been accepted for inclusion in Physics and Astronomy Faculty Publications by an authorized administrator of UKnowledge. For more information, please contact [UKnowledge@lsv.uky.edu](mailto:UKnowledge@lsv.uky.edu).

---

**Authors**

R. H. Rubin, P. G. Martin, R. J. Dufour, Gary J. Ferland, J. A. Baldwin, J. J. Hester, and D. K. Walter

**Temperature Variations and N/O in the Orion Nebula from *HST* Observations****Notes/Citation Information**

Published in *The Astrophysical Journal*, v. 495, no. 2, p. 891-904.

© 1998. The American Astronomical Society. All rights reserved. Printed in the U.S.A.

The copyright holder has granted permission for posting the article here.

**Digital Object Identifier (DOI)**

<http://dx.doi.org/10.1086/305326>

## TEMPERATURE VARIATIONS AND N/O IN THE ORION NEBULA FROM *HST* OBSERVATIONS<sup>1</sup>

R. H. RUBIN,<sup>2,3</sup> P. G. MARTIN,<sup>4</sup> R. J. DUFOUR,<sup>5</sup> G. J. FERLAND,<sup>6</sup> J. A. BALDWIN,<sup>7</sup>  
J. J. HESTER,<sup>8</sup> AND D. K. WALTER<sup>9</sup>

Received 1997 July 11; accepted 1997 October 17

### ABSTRACT

Using the Goddard High Resolution Spectrograph (GHRS) and the Faint Object Spectrograph (FOS) on the *Hubble Space Telescope*, we measured the flux of the N II] ( $2s2p^3\ ^3S_2 \rightarrow 2s^22p^2\ ^3P_{2,1}$ ) lines at  $\lambda_{\text{vac}} = 2143.45, 2139.68$  Å in the Orion Nebula—the first detection of these lines in an H II region. In order to assess the  $N^+/O^+$  ratio, we also measured the flux of the [O II] ( $2p^3\ ^2P_{1/2,3/2}^o \rightarrow 2p^3\ ^4S_{3/2}^o$ ) lines at  $\lambda_{\text{vac}} = 2471.05, 2471.12$  Å. In addition, with the FOS, other emission lines were measured in the same aperture in order to assess the average electron temperature and mean-square temperature variation ( $t^2$ ) in the  $N^+$  region, as well as the  $N^+/O^+$  ratio. When we require that the empirically determined values be equal for  $(N^+/O^+)_{\text{uv}}$  (obtained from the N II] 2142 and [O II] 2471 lines) and  $(N^+/O^+)_{\text{opt}}$  (obtained from the [N II] 6585 and [O II] 3728 lines), we obtain the following. For the ( $N^+, O^+$ ) zone, the average electron density is  $\sim 7000$  cm<sup>-3</sup>, the average electron temperature is 9500 K,  $t^2 = 0.032$ , and  $N^+/O^+ = 0.14$ .

By comparing our FOS observations to predicted fluxes, utilizing our two previous photoionization models, we are able to derive the N/O ratio. There is fairly good agreement between  $(N/O)_{\text{uv}}$  and  $(N/O)_{\text{opt}}$  as derived from the two models with a range between 0.13 and 0.18. This range also encompasses our model-derived values for  $(N/O)_{\text{ir}}$  (0.17–0.18), which fit the observed far-infrared line ratio [N III] 57  $\mu\text{m}$ /[O III] 52  $\mu\text{m}$ . The empirically derived  $N^+/O^+$  value requires a correction for the possibility that the  $N^+$  and  $O^+$  regions are not identical. Our overall results place the gas-phase Orion N/O ratio in the range 0.13–0.18, which is somewhat higher than solar.

*Subject headings:* ISM: abundances — ISM: atoms — ISM: H II regions —  
ISM: individual (Orion Nebula)

### 1. INTRODUCTION

Although quantitative nebular spectroscopy is a mature field, several fundamental problems and uncertainties have recently emerged (e.g., Liu et al. 1995). Among the more perplexing is evidence for variations in electron temperature ( $T_e$ ) resulting in large mean-square temperature fluctuations ( $t^2$ ) in nebulae (Peimbert 1967). A modest  $t^2$  can have a major (0.5 dex) impact on estimates of heavy element abundances. For comprehensive reviews regarding H II regions, see, e.g., Peimbert (1993) and Mathis (1995). Gas within the  $O^{++}$  region of a photoionized cloud is predicted to be nearly isothermal; thus, large  $t^2$  was not thought physically possible (Harrington et al. 1982; Mihalszki & Ferland 1983; Kingdon & Ferland 1995; Maciejewski, Mathis, & Edgar 1996). However, observations of Orion (Peimbert, Storey, & Torres-Peimbert 1993) and the planetary nebula (PN) NGC 7009 (Liu et al. 1995) allowed careful comparison between

abundances measured from faint recombination lines and from the classical forbidden lines. These imply that  $t^2$  is large and has caused the abundances of C, N, and O to be underestimated by factors of 2–5. The question of the existence of large  $t^2$  is a key one in nebular astrophysics today; it would bring into question all emission-line abundance studies.

Another uncomfortable situation exists regarding the N/O abundance ratio that has been derived for Galactic H II regions, including Orion. This ratio as inferred from the  $N^{++}/O^{++}$  ratio using far-infrared (FIR) lines has been significantly higher than what is obtained from the  $N^+/O^+$  ratio using optical lines. The FIR method used the [O III] (52, 88  $\mu\text{m}$ ) and [N III] 57  $\mu\text{m}$  lines (e.g., Lester et al. 1987; Rubin et al. 1988; Simpson et al. 1995), while the optical method used the [O II] ( $\lambda_{\text{air}} = 3726, 3729$  Å) and [N II] 6584 Å lines (e.g., Shaver et al. 1983). Specifically for the Orion Nebula, N/O from the  $N^{++}/O^{++}$  ratio is  $\sim 0.2$  (Rubin et al. 1991a; Baldwin et al. 1991), nearly a factor of 2 higher than N/O inferred from  $N^+/O^+$  (e.g., Walter, Dufour, & Hester 1992). Orion is one of just a few H II regions for which the comparison may be made for roughly the same nebular position.

The N/O ratio is of special interest in the context of galactic chemical evolution and stellar nucleosynthesis (for reviews, see Wheeler, Sneden, & Truran 1989; Vila-Costas & Edmunds 1993). Conventional stellar structure and nucleosynthesis theory indicates that nitrogen enrichment arises from both primary and secondary production in stars, while oxygen enrichment occurs from only primary nucleosynthesis in massive stars (cf. Vila-Costas & Edmunds 1993, and references therein). For intermediate-mass stars, nitrogen is produced from the CN cycle, being secondary if

<sup>1</sup> Based on observations made with the NASA/ESA *Hubble Space Telescope*, obtained at STScI, which is operated by AURA, Inc., under NASA contract NAS 5-26555.

<sup>2</sup> NASA/Ames Research Center, Moffett Field, CA 94035-1000.

<sup>3</sup> Orion Enterprises.

<sup>4</sup> Canadian Institute for Theoretical Astrophysics, University of Toronto, Toronto, ON, Canada M5S 3H8.

<sup>5</sup> Rice University, Department of Space Physics and Astronomy, Box 1892, Houston, TX 77251-1892.

<sup>6</sup> University of Kentucky, Department of Physics and Astronomy, Lexington, KY 40506.

<sup>7</sup> Cerro Tololo Inter-American Observatory, Casilla 603, La Serena, Chile.

<sup>8</sup> Arizona State University, Department of Physics and Astronomy, Tempe, AZ 85287.

<sup>9</sup> South Carolina State University, Physical Sciences, Box 7296, Orangeburg, SC 29117.

the carbon preexisted the star's formation, or primary if the carbon came from the products of He burning that were dredged-up into the H-burning shell. Observations of metal-poor irregular galaxies give  $N/O \approx 0.034$ , varying little with  $O/H$ . While the simplest chemical evolution scenario would suggest that such follows as the ratio of the primary yields of O and N in massive stars, theoretical work has not developed a mechanism for producing such a high yield of primary N in massive stars. Vila-Costas & Edmunds show that such a flat variation in  $N/O$  with  $O/H$  in metal-poor galaxies could be explained if the time delay for the primary N production in intermediate-mass stars were only of the order of 100 Myr. However, in the H II regions of more metal-rich galaxies, for which  $12 + \log(O/H) > 8.0$ ,  $N/O$  is observed to increase with  $O/H$ , indicating a secondary yield of nitrogen from intermediate-mass stars that is proportional to  $O/H$  (and also time-delayed) in the chemical evolution of galaxies. Moreover, in Galactic and extragalactic H II regions, we find significant variations in  $N/O$  at a given  $O/H$  between galaxies and among H II regions of a given galaxy, which might be due to variations in the local star formation history, infall effects, variable IMFs, or just observational/computational inaccuracies. Therefore, determination of accurate  $N/O$  values in Orion and other Galactic and extragalactic H II regions is important to determine the chemical evolutionary "age" of the interstellar medium (ISM), as well as to accurately determine the extent of variations of  $N/O$  with  $O/H$  indicative of other processes which affect  $N/O$ .

We address the issue of  $T_e$  fluctuations as well as the  $N/O$  ratio in the Orion Nebula using *HST* observations. Much of this work is made possible by our measurements of the  $N \text{ II}]$  ( $2s2p^3 \ ^5S_2 \rightarrow 2s^22p^2 \ ^3P_{2,1}$ ) lines at  $\lambda_{\text{vac}} = 2143.45, 2139.68 \text{ \AA}$ , in sum referred to as  $2142 \text{ \AA}$ .<sup>10</sup> The measurement of this line in Orion is the first in an H II region. Previously it has been seen in RR Tel (Penston et al. 1983), nova CrA 1981 (Williams et al. 1985), the  $\eta$  Car S condensation (Davidson et al. 1986), and planetary nebulae (Vassiliadis et al. 1996). The line has also been seen in emission in the Earth's aurora and dayglow (e.g., Bucselo & Sharp 1989, and references therein). The red component is expected to be a factor of 2.31 stronger than the blue one (J. Fuhr, private communication 1997).

In § 2 we present the *HST* observations. Section 3 contains an empirical interpretation of the data, including analyses in terms of  $T_e$  and  $t^2$ , as well as the  $N/O$  ratio. Section 4 presents an analysis using photoionization models. In § 5 we provide a discussion and conclusions.

## 2. *HST* OBSERVATIONS

From our earlier Cycle 3 Faint Object Spectrograph (FOS) data, we combined spectra taken at three positions in the Orion Nebula in order to maximize the S/N for identification of faint lines in the UV (Rubin et al. 1995). These positions, as well as others we mention here, are shown in an earlier paper (see Fig. 1 [Pl. 1] in Rubin et al. 1997). The feature at  $2142 \text{ \AA}$  was identified as emission from the blended pair of  $N \text{ II}]$  lines. Subsequently, we were granted FOS Cycle 5 time for, among other things, further study of the  $2143.45, 2139.68 \text{ \AA}$  lines. We were also granted time for deep high-resolution spectroscopy of this wavelength region

with the Goddard High Resolution Spectrograph (GHRS). In an attempt to maximize the strength of these  $N \text{ II}]$  lines, we utilized the WFPC2 imagery of Orion (from C. R. O'Dell's observations), primarily those taken with F658N. Consequently, we defined FOS-1SW, a circular aperture of  $0''.86$  diameter, as a Cycle 5 FOS target. Its center is at  $(\alpha, \delta) = (05^{\text{h}}35^{\text{m}}14^{\text{s}}.71, -05^{\circ}23'41''.5)$  (equinox J2000),  $18''.5$  south and  $26''.2$  west of  $\theta^1$  Ori C. The GHRS-1SW aperture is the  $1''.74$  square Large Science Aperture (LSA) centered at the same position as FOS-1SW, with its orientation determined by the time of the actual observation (see Fig. 1 in Rubin et al. 1997).

### 2.1. FOS Observations

We observed with FOS on 1995 October 23–24 (UT) using the  $0''.86$  diameter circular aperture. Spectra were taken with gratings G190H, G270H, G400H, G570H, and G780H, which provide total coverage from about  $1650\text{--}7800 \text{ \AA}$ . Data for the  $N \text{ II}]$   $2139.68, 2143.45 \text{ \AA}$  lines were obtained by co-adding two G190H spectra of 790 and 2170 s; an Earth occultation period necessitated the splitting of exposures. Each exposure was done in ACCUMULATION mode. The other spectra were made with the following (exposure/mode): G270H (1320 s/ACCUM), G400H (301 s/RAPID), G570H (225 s/RAPID). (G780H is not discussed further, because we do not directly use those line measurements here.)

The data products delivered to us underwent the standard pipeline version of "calfos." Considerably later, possible calibration problems that could affect our data were described in the STScI Analysis Newsletter, STAN-FOS 9, 1996 March. We were advised by STScI/FOS personnel that the worst case will be for the G190H grating, where a count/flux change can be as much as  $\sim 5\%$ – $7\%$ . We were told that the other gratings will have less change, with the G400H suffering the least. Because of the importance of the  $N \text{ II}]$   $2142 \text{ \AA}$  line here, we requested a recalibration of all our G190H spectra. We are grateful to Jeffrey Hayes of STScI for providing this service.

Figure 1 displays the portion of the spectrum that con-

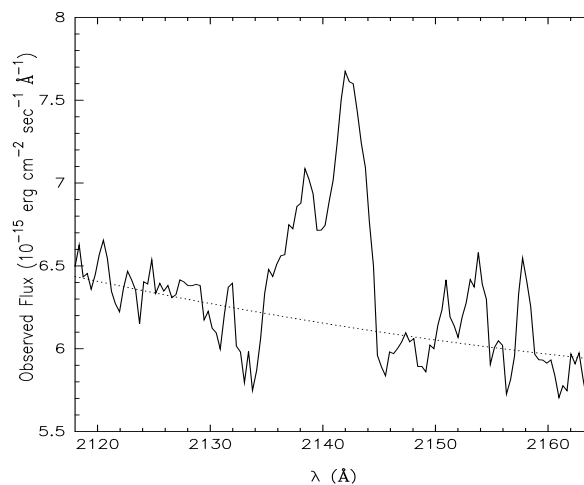


FIG. 1.—Portion of the pipeline-calibrated FOS/G190H spectrum of the Orion Nebula observed with the *HST* at position FOS-1SW, showing the partially blended  $N \text{ II}]$   $2139.68, 2143.45 \text{ \AA}$  lines. For display, we have applied a three-point boxcar smoothing to the spectrum. Dotted line indicates a quadratic continuum fit over the extended interval  $2070\text{--}2210 \text{ \AA}$  excluding the line. The net flux is determined from the area above the fitted continuum. The flux scale here has not been adjusted for the extended-source and grating corrections (a combined factor of 0.855) discussed in the text.

<sup>10</sup> Unless stated otherwise, all wavelengths used in this paper for identification of lines are on the vacuum scale (which may make some appear strange, as they are often used on the air wavelength scale).

TABLE 1  
FOS<sup>a</sup> AND GHRS<sup>b</sup> SPECTRAL LINES AT POSITION 1SW IN THE ORION NEBULA

ID (1)	G <sup>d</sup> (2)	WAVELENGTH		FWHM (Å) (5)	FLUX IN APERTURE <sup>c</sup>			Relative to H $\beta$ (9)	I <sup>h</sup> (10)
		Measured (3)	Vacuum (4)		Pipeline <sup>e</sup> (6)	Observed <sup>f</sup> (7)	Corrected <sup>g</sup> (8)		
N II] .....	1	...	2142 <sup>i</sup>	...	0.078 ± 0.006	0.067	0.530	1.898	0.912
[O II] .....	2	2470.64	2471 <sup>i</sup>	4.31	0.886 ± 0.007	0.774	4.653	16.68	8.010
[O II] .....	3	3725.86	3728 <sup>i</sup>	6.94	9.132 ± 0.029	8.242	41.43	148.5	71.32
H $\gamma$ .....	3	4339.66	4341.69	6.33	3.376 ± 0.016	3.047	13.81	49.51	23.77
[O III] .....	3	4362.41	4364.44	6.33	0.082 ± 0.013	0.074	0.332	1.189	0.571
H $\beta$ .....	4	4861.07	4862.69	9.09	7.605 ± 0.062	6.936	27.90	100.0	48.03
[O III] .....	4	5006.49	5008.24	9.12	22.00 ± 0.219	20.06	78.25	280.5	134.7
[N II] .....	4	5753.53	5756.24	9.99	0.152 ± 0.007	0.138	0.468	1.679	0.806
[N II] .....	4	6547.34	6549.86	9.48	3.162 ± 0.168	2.884	8.562	30.69	14.74
H $\alpha$ .....	4	6562.11	6564.63	9.48	28.58 ± 0.202	26.06	77.20	276.7	132.9
[N II] .....	4	6582.71	6585.23	9.48	9.151 ± 0.174	8.346	24.64	88.32	42.42
[S II] .....	4	6715.51	6718.32	8.62	0.372 ± 0.012	0.339	0.979	3.510	1.686
[S II] .....	4	6729.50	6732.71	8.62	0.753 ± 0.013	0.687	1.980	7.097	3.409
N II] .....	5	2139.888	2139.68	0.641	0.055 ± 0.007	0.052	0.412	...	0.136
N II] .....	5	2143.623	2143.45	0.641	0.145 ± 0.008	0.138	1.095	...	0.362
[O II] .....	5	2471.253	2471 <sup>i</sup>	0.603	3.602 ± 0.060	3.422	20.56	...	6.791

<sup>a</sup> FOS 0.86 diameter circular aperture.

<sup>b</sup> GHRS 1.74 square aperture.

<sup>c</sup> In units of  $10^{-13}$  ergs cm<sup>-2</sup> s<sup>-1</sup>.

<sup>d</sup> Gratings: 1: G190H; 2: G270H; 3: G400H; 4: G570H; 5: G270M (GHRS).

<sup>e</sup> From pipeline with 1  $\sigma$  statistical (only) uncertainty.

<sup>f</sup> Corrected for optics as per *HST* Handbook (1995); see § 2.1 and 2.2.

<sup>g</sup> Further corrected for extinction.

<sup>h</sup> Surface brightness in units of  $10^{-13}$  ergs cm<sup>-2</sup> s<sup>-1</sup> arcsec<sup>-2</sup>.

<sup>i</sup> For sum of a line pair: 2139.68 and 2143.45 Å; 2471.05 and 2471.12 Å; 3727.09 and 3729.88 Å.

tains the partially blended N II] lines. The flux of the line pair is most readily and reliably determined by direct integration of the area above a fitted quadratic continuum. This is similar to direct integration with the IRAF<sup>11</sup> ONEDSPEC:SPLIT software using the *e*-option. This flux is entered in column (6) of Table 1, labeled "Pipeline." The 1  $\sigma$  statistical uncertainty in the line flux is about 7%. This was estimated via confidence intervals of the one-dimensional marginalized distributions of the areas of Gaussian components within a nonlinear least-squares fitting program, from the quality of fit to the original unsmoothed data. (In this particular model, the Gaussian components were constrained to have the same FWHM, known separation 3.77 Å, and theoretical flux ratio 2.31 obtained using the current *A*-values; Appendix A.) For this low-S/N line (pair), this statistical error is larger than the expected systematic errors—about 1% from the flat fielding and 3% from the flux calibration (*HST* Data Handbook).

Table 1 also lists our measured FOS fluxes for several other lines that we shall use in this paper, including the [O II] ( $2p^3\ ^2P_{1/2,3/2}^o \rightarrow 2p^3\ ^4S_{3/2}^o$ ) lines at  $\lambda_{\text{vac}} = 2471.05, 2471.12$  Å. These have been determined using the IRAF Gaussian fitting routines (using linear baselines for the continuum). Sets of lines with the same FWHM in the table were measured together with the deblend (*d*)-option (e.g., [S II] 6718, 6733). Each line group was fitted simultaneously using a fixed (known) wavelength separation, a common wavelength shift, and a common FWHM. These Gaussian fits were checked using our own program, which also supplies the statistical errors tabulated. For the brighter lines, the systematic errors dominate.

Column (7) of Table 1 contains what we term the observed flux. We have applied a grating-dependent correction factor for extended sources to the pipeline calibrated

spectrum (see *HST* Data Handbook 1995, pp. 286–287). Column (8) shows the extinction-corrected fluxes. The extinction corrections are based on our observed FOS data for Balmer, He I, and [O II] emission lines at this position FOS-1SW. This set of corrections is consistent with the shape of the extinction curve derived from observations of the Orion Trapezium stars (Martin et al. 1998). Columns (9) and (10) provide extinction-corrected fluxes relative to H $\beta$  (value 100) and surface brightness, respectively.

## 2.2. GHRS Observations

We observed with GHRS on 1995 October 14–15 (UT) with the G270M grating, using the LSA centered on position FOS-1SW. Because this paper is part of a larger study of the Orion Nebula with *HST* to be presented elsewhere, we limit our presentation of data in the figures below to portions relevant to the matters at hand. The spectral resolution is  $\sim 0.1$  Å for a point source (Table 8-1 and Fig. 8-1 of Soderblom et al. 1995). For a uniformly filled LSA, there are 8 diodes illuminated, which is expected to cause a degradation in resolving power by a factor of 8. This is borne out by observations of geocoronal Ly $\alpha$  (see § 3 in Conti, Leitherer, & Vacca 1996). Hence, in the limit of a uniformly filled LSA, lines with FWHM  $\sim 0.8$  Å could be expected.

For the [O II] 2471 Å blended lines the grating was centered at 2480.8 Å in the  $\sim 47.3$  Å bandpass. The exposure was 381 s in ACCUMULATION mode. When the line is fitted as a single Gaussian (Fig. 2a shows the unsmoothed data and the fit), the measured flux for the blended pair is  $3.8 \times 10^{-13}$  ergs cm<sup>-2</sup> s<sup>-1</sup>, the line center wavelength is 2471.254 Å, and the (instrumental) FWHM = 0.603 Å (73 km s<sup>-1</sup>). Because of the spectral impurity introduced by the LSA, the line profiles have flatter tops and less extended bases (are more "trapezoidal") than the Gaussian fits. It is also apparent that the Gaussian fit is overestimating the line

<sup>11</sup> IRAF is distributed by NOAO, which is operated by AURA, under cooperative agreement with the NSF.

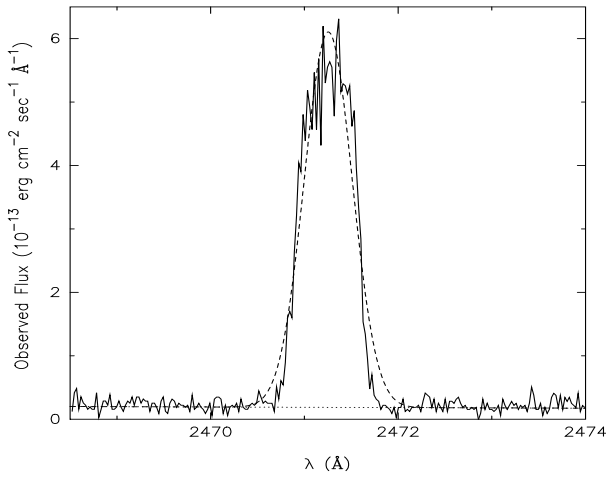


FIG. 2a

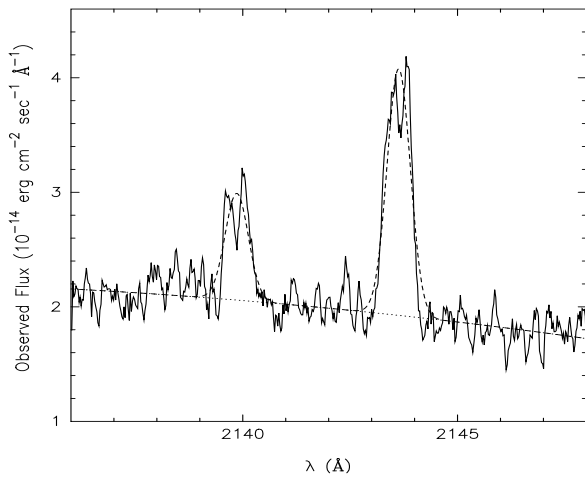


FIG. 2b

FIG. 2.—Portions of the GHRS pipeline-calibrated spectra of the Orion Nebula at position GHRS-1SW. The flux here has not been adjusted for the factor of 0.95 discussed in the text. (a) Blended [O II] 2471.05, 2471.12 Å lines (unsmoothed). A single Gaussian plus a linear continuum fit to the data are shown. (b) Resolved N II] 2139.68, 2143.45 Å lines. For this display (not the flux determination) a five-point boxcar smoothing has been applied. Gaussian components plus a quadratic continuum fit to the data are shown (see text).

flux. The flux measured with the *e*-option is  $3.6 \times 10^{-13}$  ergs  $\text{cm}^{-2} \text{s}^{-1}$  (5.3% smaller), and the line centroid is at wavelength 2471.253 Å. This is the approach that we adopt as preferable (see entry in Table 1).

The flux represents an integrated value over the LSA. Because the measured line width is much closer to the uniformly filled LSA limit than to the point-source limit, we have multiplied the fluxes that result from the standard pipeline GHRS calibration (“calhrs”) by 0.95 (recommended for a uniformly filled LSA; *HST* Data Handbook 1995, p. 377). Table 1 also has extinction-corrected fluxes. These corrections are based on our FOS data as described above.

The relative contributions of the two components to the observed [O II] blend may be estimated. According to the nebular model of Rubin et al. (1991a), the ratio of intensities,  $I(2471.12)/I(2471.05) = 3.97$  and is nearly invariant with position in the model. When we use this relative weighting to derive the expected vacuum wavelength, we obtain 2471.106 Å. The difference from the observed centroid

wavelength is 0.147 Å, corresponding to  $V_{\text{helio}} = 17.8 \text{ km s}^{-1}$ , in agreement with the  $\sim 17 \pm 2 \text{ km s}^{-1}$  from emission lines arising in the main ionization zone (O’Dell et al. 1993).

For the N II] line pair, the grating was centered at 2150.89 Å, and the bandpass was  $\sim 48.5 \text{ Å}$ . The exposure was 6854 s in ACCUMULATION mode. With the enormous improvement that the GHRS spectrum provides in higher resolution, both N II] lines are prominent (Fig. 2b). Again there is a clear departure in the line profile from the Gaussian shape in the direction of the trapezoidal shape.<sup>12</sup>

The line fluxes were determined using both Gaussian fitting (*d*-option) and direct integration (*e*-option) to measure the net line flux above the continuum. The Gaussian fit to the data shown in Figure 2b is obtained by requiring that the known separation in  $\lambda_{\text{vac}}$  between the two lines be maintained. There is only a single degree of freedom in the wavelength direction. Additionally, we force a single (unknown) FWHM for both lines, as the width is set by instrumental resolution (see above) and not the intrinsic width. The best-fitting FWHM = 0.64 Å (90  $\text{km s}^{-1}$ , within the uncertainty being the same as for the [O II] blend). Finally, the fit provides the best linear continuum baseline.

The line fluxes by the preferred approach, the *e*-routine, are  $1.45$  and  $0.55 \times 10^{-14}$  ergs  $\text{cm}^{-2} \text{s}^{-1}$  for the red and blue components, respectively (Table 1). (These fluxes are again somewhat lower than from the two-line Gaussian fit, though within the statistical measurement errors found from our Gaussian fits as described above.) The ratio of the flux of the 2143 Å line to that of the 2140 Å line is 2.6, which agrees with the theoretical value of 2.31 within the statistical errors.

With the *e*-option measurements for N II], the line center wavelengths are 0.173 and 0.208 Å redward of the 2143.45 (stronger line) and 2139.68 Å vacuum rest wavelengths, respectively, corresponding to  $V_{\text{helio}} = 24.1$  and 29.1  $\text{km s}^{-1}$ . With the constrained Gaussian simultaneous fit, the line center wavelengths are  $0.180 \pm 0.013 \text{ Å}$  redward of the vacuum rest wavelengths, like the weighted average of the above. This corresponds to  $V_{\text{helio}} = 25.1 \pm 1.8 \text{ km s}^{-1}$ , rather different than the  $\sim 17 \pm 2 \text{ km s}^{-1}$  characteristic of the main ionization zone or from [O II] above. It is possible that the statistical errors derived from fitting Gaussian components underestimate the true uncertainty, given the limitations of this model fit to the line profiles (Fig. 2b). As noted above, the line profiles are noisy, though perhaps no more than expected from the level of noise in the continuum. The finite size of the LSA is also relevant. Recall that the point-source line width is broadened from about 0.1 Å to the observed  $\sim 0.6 \text{ Å}$  (closer to a more uniformly illuminated aperture). Therefore spatial structure in the nebular surface brightness across the LSA aperture, in the direction of the dispersion, could induce structure in the line profile and/or an apparent Doppler shift.

### 3. EMPIRICAL INTERPRETATION OF THE *HST* DATA

The acquisition of these lines (several using FOS, with the same aperture) permits us to address  $T_e$  and  $t^2$  along the

<sup>12</sup> Although the spectrum is noisy, one might wonder if the central dips in both of the lines could be caused by self-absorption. It can be shown that the optical depth  $\tau$  should be less than 0.002 and 0.0009 for the 2143 and 2140 lines, respectively. The calculation uses the thermal width only; thus, velocity broadening will make  $\tau$  even lower. We thank X.-W. Liu for help here. Another decisive argument against self-absorption is that the apparent central inversion is relatively larger in the weaker line.

specific column through the  $N^+$  region. With this information, we can also derive the  $N^+/O^+$  ratio by more than one method. In the subsections that follow, we utilize atomic data—electron impact collision strengths and spontaneous emission probabilities (Einstein  $A$ -values)—to solve the  $N^+$  energy level populations. See Appendix A for details of the data adopted, including those for  $O^+$  needed later. We refer to the levels in ascending order of energy; for  $N^+$ , these are levels 1–6,  $^3P_0$ ,  $^3P_1$ ,  $^3P_2$ ,  $^1D_2$ ,  $^1S_0$ , and  $^5S_2$ .

### 3.1. Electron Temperature ( $T_e$ ) and $T_e$ Variations from Lines of $N^+$

The observations of lines that arise from levels 4, 5, and 6 of  $N^+$  permit us to investigate the populations of levels with widely different excitation temperatures, and hence their sensitivities to  $T_e$ . We treat the combined emission (2142 Å) from level 6, the 5756 Å line from level 5, and the 6585 Å line from level 4. Although Table 1 includes our measurement of the 6550 Å line (arising from level 4), we do not use it in this analysis, because it is weaker than 6585 and closer in wavelength to  $H\alpha$  at 6565 Å than is the 6585 line, causing much more uncertainty in its FOS flux measurement.

Following Peimbert (1967), we may write the flux ratios in a set of equations that utilize a Taylor series expansion about an average electron temperature  $T_X$ , defined by

$$T_X = \frac{\int T_e N_e N(N^+) dV}{\int N_e N(N^+) dV}, \quad (1)$$

and retain terms to second order. These involve terms containing  $t_X^2$ , the mean-square temperature variation, given by the following equation when  $n = 2$ :

$$t_X^n = \frac{\int (T_e - T_X)^n N_e N(N^+) dV}{T_X^n \int N_e N(N^+) dV}. \quad (2)$$

The integration in equations (1) and (2) is over the column defined by the aperture, along the line of sight. Then for the 2142 to 5756 flux ratio,

$$\frac{F_{2142}}{F_{5756}} = \frac{K_6}{K_5} \exp\left(-\frac{20284}{T_X}\right) C_{\text{tvar}}. \quad (3)$$

In the above equation,  $(K_6/K_5) \exp(-20284/T_X) = \epsilon_{2142}/\epsilon_{5756}$ , where  $\epsilon_\lambda$  is the normalized volume emissivity, written in terms of the volume emissivity for the line  $j_\lambda$  as  $\epsilon_\lambda \equiv j_\lambda/(N_e N_i)$ .  $N_i$  is the relevant ion density.  $\epsilon_\lambda$  depends on the level populations only. It is helpful to “factor out” the differential Boltzmann factor dependence in equation (3), as well as in equations (6) and (7) later. The energy levels used in the above equation, as well as those used throughout this paper, are discussed in Appendix A.

We follow the technique in Peimbert (1967), Rubin (1969), and notation of Rubin et al. (1988, p. 381) to write the correction factor for  $T_e$  variations ( $C_{\text{tvar}}$ ) as

$$C_{\text{tvar}} = \frac{1 + b_{\lambda 1} t_X^2}{1 + b_{\lambda 2} t_X^2}, \quad (4)$$

where subscripts  $\lambda 1$  and  $\lambda 2$  refer to the respective  $b$ -values for the pertinent lines—2142 and 5756 Å in the case of equation (3)—and

$$b_\lambda = \frac{1}{2}[(\chi/kT_X)^2 - 3(\chi/kT_X) + \frac{3}{4}]; \quad (5)$$

$\chi$  is the excitation energy above ground for the upper level of the transition. Similarly, forming the other flux ratios, we

arrive at equations (6) and (7).

$$\frac{F_{5756}}{F_{6585}} = \frac{K_5}{K_4} \exp\left(-\frac{24993}{T_X}\right) C_{\text{tvar}}, \quad (6)$$

$$\frac{F_{2142}}{F_{6585}} = \frac{K_6}{K_4} \exp\left(-\frac{45277}{T_X}\right) C_{\text{tvar}}. \quad (7)$$

The evaluation of  $T_X$  from equations (3), (6), and (7) is done by solving the statistical equilibrium for the six-level populations. Because the  $K$ s depend on  $N_e$  and the temperature being solved for, the solution is iterative.

The expression for  $b_\lambda$  in equation (5) is valid in the low-density limit. As in the original paper (Peimbert 1967), the volume emissivities are assumed to be proportional to  $T_e^{-0.5} \exp(-\chi/kT_e)$ —the low-density limit functional form. This permits an analytical treatment of the Taylor series expansion, including the second-order term that involves the second derivative of the normalized volume emissivity with respect to temperature; this is related to  $b_\lambda$ . For the lines of  $N^+$  used and the results found here for Orion,  $N_e$  is well below each critical density ( $N_{\text{crit}}$ ) for the respective energy levels: level 4,  $6.8 \times 10^4$ ; level 5,  $1.5 \times 10^7$ ; and level 6,  $1.8 \times 10^9 \text{ cm}^{-3}$  (for  $T_e = 9500 \text{ K}$ ). Hence, the analytical treatment in the low-density limit should be valid for the  $N^+$  lines. On the other hand, for  $O^+$  lines (used later) arising from levels 2 (3730 Å) and 3 (3727 Å),  $N_{\text{crit}} = 2500$  and  $4700 \text{ cm}^{-3}$ . Thus, when using these for analysis, we need to be cognizant of possible limitations resulting from collisional deexcitations. In principle, the Taylor series procedure used should not be restricted to being able to handle only the low-density limit. The restriction may be circumvented by replacing the analytical treatment with a numerical one. We plan to describe this fully in a future paper. Preliminary results using that more general, numerical formulation show that the conclusions reached here using the low-density limit analytical treatment are reliable and are not going to be significantly revised.

It is sometimes useful to approximate the  $K$ s in equations (3), (6), and (7) for the case in which collisional deexcitations are small. The  $K$ s in these equations can be evaluated in terms of the atomic data; then,

$$K_6/K_5 = 8.51/(1 + 0.1705x), \quad (8)$$

$$K_5/K_4 = 0.1816(1 + 0.3375x), \quad (9)$$

and

$$K_6/K_4 = 1.545(1 + 0.3375x)/(1 + 0.1705x), \quad (10)$$

where  $x = 0.01N_e/(T_e)^{1/2}$ . Equations (8)–(10) should be usable as long as collisional deexcitation is small. Their accuracy is thus better at small values of  $x$ . We do not use such approximations in this paper; instead, we deal explicitly with the normalized volume emissivities for the lines.

To test the validity of applying the above procedure, we used simple cases having  $T_e$  vary linearly with position. In order to make these tests a pure determination of the adequacy of the Taylor series representation for the line fluxes, we kept all densities and ionic abundances constant. We set  $N_e = 1 \text{ cm}^{-3}$  to insure that all lines are well below their respective  $N_{\text{crit}}$  in order to validate the procedure using the Taylor series expansion to second order with the analytical expression for  $\epsilon_\lambda$  (low-density limit). At each position, the volume emissivities are computed for the lines of interest here. These are then summed along the path to produce a total flux in those lines. In this way we generate

“observables” for the  $F_{6585}$ ,  $F_{5756}$ , and  $F_{2142}$  fluxes. We also calculate analytically the appropriate  $T_X$ ,  $t_X^2$ , and  $t_X^4$  for this linear path. The expressions for  $t_X^3$  and  $t_X^4$  are obtained from equation (2), substituting  $n = 3$  and 4. For our linear cases,  $t_X^3 = 0$ . Next we take these generated fluxes and use them in equations (3), (6), and (7) as if they were real observations. These are solved numerically and may be visualized with the graphical aid of Figure 3. There is one redundant line ratio among the three used; this provides a good numerical check in that there should be a common solution of equations (3), (6), and (7) at the same intersection. Finally, the reliability of the intersection solution is gauged by how well it agrees with the analytical  $T_X$  and  $t_X^2$ , which is marked in the figures.

We present test cases that result in inferred values for  $T_X$  and  $t_X^2$  that are close to what we find below from the Orion data. This will prove helpful in guiding the interpretation of the actual Orion results. Figures 3a, 3b, and 3c are meant to illustrate three types of behavior. Case I (Fig. 3a) represents the situation in which there are solutions to equations (3), (6), and (7). Here  $T_e$  varies linearly from 6500–12500 K and results in  $T_X = 9500$  K,  $t_X^2 = 0.033241$ , and  $t_X^4 = 0.0019889$  analytically. The solution obtained from applying equations (3), (6), and (7) to the generated “observed line fluxes” is at  $T_X = 9446$  K,  $t_X^2 = 0.034121$ . The x-intercepts of the lines represent  $T_e$  that would be derived by ignoring temperature variations ( $t_X^2 = 0$ ):  $T_{65} = 10,684$  K (subscript denotes energy levels from which lines arise);  $T_{64} = 10380$

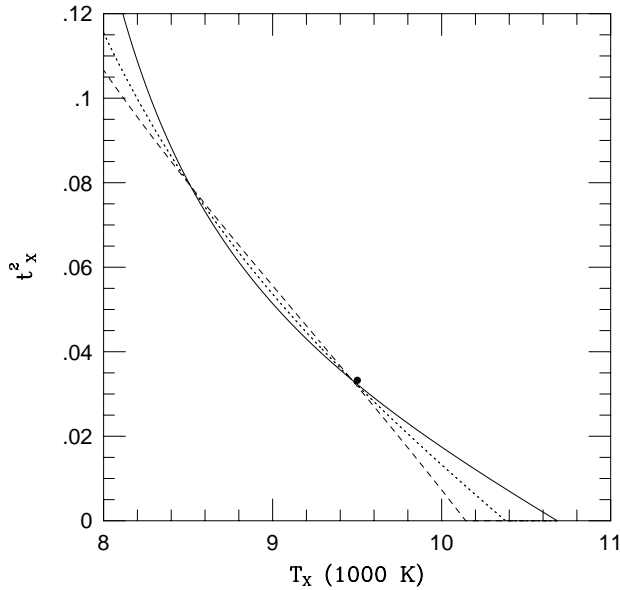


FIG. 3a

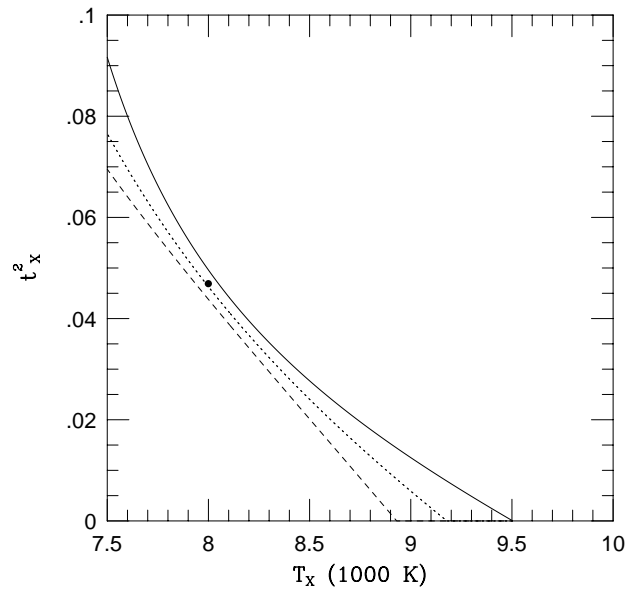


FIG. 3b

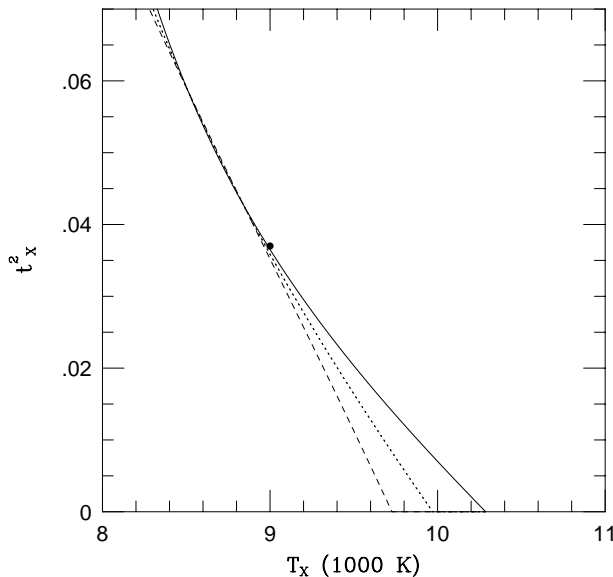


FIG. 3c

FIG. 3.—Loci of solutions for each of equations (3), (6), and (7) (solid, heavy-dashed, and small-dashed lines, respectively) for three test cases. Where these lines cross the x-axis is the  $T_e$  value that would be inferred for each equation in the absence of  $T_e$  fluctuations. (a) Case I: Intersection of the loci at  $T_X = 9446$  K,  $t_X^2 = 0.034121$  is the desired solution. This agrees well with the analytical result of  $T_X = 9500$  K,  $t_X^2 = 0.033241$  (filled point). The intersection of the curves at another point (8546 K, 0.07690) is a spurious solution discussed in the text. (b) Case II: There is no solution, as indicated by the lack of any intersection. The analytical result is  $T_X = 8000$  K,  $t_X^2 = 0.046875$  (filled point). (c) Case III: “Transition” situation (see text). The intersection of the loci at  $T_X = 8766$  K,  $t_X^2 = 0.045909$  is the desired solution. This may be compared to the analytical result of  $T_X = 9000$  K,  $t_X^2 = 0.037037$  (filled point).

K; and  $T_{54} = 10143$  K. There is also a spurious solution, physically, represented by the second intersection at lower  $T_X$  and higher  $t_X^2$ .

**Case II** (Fig. 3b) represents the situation in which there are no solutions to equations (3), (6), and (7). This test case has  $T_e$  varying linearly from 5000–11,000 K and results in  $T_X = 8000$  K,  $t_X^2 = 0.046875$ , and  $t_X^4 = 0.0039551$  analytically. The  $(T_X, t_X^2)$  point is marked in Fig. 3b. Finally, **Case III** (Fig. 3c) is meant to represent the transition situation between the other two situations. Here there is just one solution, as the loci for equations (3), (6), and (7) just touch at a point before diverging again. This test case has  $T_e$  varying linearly from 6000–12,000 K and results in  $T_X = 9000$  K,  $t_X^2 = 0.037037$ , and  $t_X^4 = 0.0024691$  analytically. The  $(T_X, t_X^2)$  point is marked Fig. 3c. This test case did not quite succeed in actually having the three loci just “tangent” at one point. It is actually like Case I in having two solutions. The physical solution is at  $T_X = 8766$  K,  $t_X^2 = 0.045909$ —at a temperature that is 234 K too low and a  $t_X^2$  that is 0.0089 too high, compared to the true values. This behavior will be referred to later with regard to interpreting the Orion results. Next, we examine both this situation and the one in which there are no solutions—situations realized at the larger  $t_X^2$  values—in view of the neglect of higher-order  $T_e$ -variation terms.

### 3.1.1. Higher-Order $T_e$ -Variation Terms

To account for higher-order terms than second order, it is necessary to modify  $C_{\text{ivar}}$  as given by equation (4). We expand the analysis to include the next two terms in the Taylor series expansion about  $T_X$ . (Here, as in § 3.1, we use the analytical treatment in the low- $N_e$  limit.) The correction factor for  $T_e$  variations is then

$$C_{\text{ivar}} = \frac{1 + b_{\lambda 1} t_X^2 + c_{\lambda 1} t_X^3 + d_{\lambda 1} t_X^4}{1 + b_{\lambda 2} t_X^2 + c_{\lambda 2} t_X^3 + d_{\lambda 2} t_X^4}, \quad (11)$$

where

$$c_{\lambda} = \frac{1}{6} \left[ \left( \frac{\chi}{kT_X} \right)^3 - 7.5 \left( \frac{\chi}{kT_X} \right)^2 + 11.25 \left( \frac{\chi}{kT_X} \right) - \frac{15}{8} \right], \quad (12)$$

and

$$d_{\lambda} = \frac{1}{24} \left[ \left( \frac{\chi}{kT_X} \right)^4 - 14 \left( \frac{\chi}{kT_X} \right)^3 + 52.5 \left( \frac{\chi}{kT_X} \right)^2 - 52.5 \left( \frac{\chi}{kT_X} \right) + \frac{105}{16} \right]. \quad (13)$$

These relations permit an understanding of why there are no intersections of loci in Figure 3b. Let us examine the errors made in  $t_X^2$  at the known analytical  $T_X$  value (8000 K) by using the second-order treatment (i.e., eq. [4]). We do this by comparing the “generated observable” line ratios that appear on the left-hand side of equations (3), (6), and (7) to the respective right-hand side calculated with the analytical  $T_X$  and  $t_X^2 = 0.046875$ . From equation (5),  $b_{2142} = 23.1517$ ,  $b_{5756} = 8.83563$ , and  $b_{6585} = 0.036729$ . The resulting values for  $t_X^2$  are then 0.049598, 0.043463, and 0.046109 from equations (3), (6), and (7), respectively, as appear graphically in Figure 3b. Now we demonstrate that for each of the three loci, the  $t_X^4$  term accounts for essentially all of these differences from the true (analytical) value. We repeat the above calculation with equation (11) instead of with equation (4). Recall that  $t_X^3$  (and all  $t_X^n$ , with odd  $n$ ) is identically zero for our straight-line functional forms. From

equation (13),  $d_{2142} = -1.9100$ ,  $d_{5756} = -5.7352$ , and  $d_{6585} = 1.0526$ . Correcting for the  $t_X^4$  term ( $t_X^4 = 0.0039551$ ), we find  $t_X^2$  is 0.046953, 0.047000, and 0.046809 from equations (3), (6), and (7)—in essential agreement with  $t_X^2(\text{analytical}) = 0.046875$ .

The same sort of analysis may be applied to Case III. Here, for  $T_X(\text{analytical}) = 9000$  K,  $b_{2142} = 17.1249$ ,  $b_{5756} = 6.18905$ , and  $b_{6585} = -0.30033$ . The resulting values for  $t_X^2$  are then 0.036487, 0.034908, and 0.035708 from equations (3), (6), and (7), respectively, as appear graphically in Figure 3c. With equation (11), we have  $d_{2142} = -7.3946$ ,  $d_{5756} = -3.5921$ , and  $d_{6585} = 0.96641$ . Correcting for the  $t_X^4$  term, we find  $t_X^2$  is 0.037216, 0.036707, and 0.036965 from equations (3), (6), and (7), in agreement with  $t_X^2(\text{analytical}) = 0.037037$ . Because the three loci in Figure 3c are slightly out of kilter as a result of not accounting for  $t_X^4$  terms, the adjustments to  $t_X^2$  result in the “solution” intersection, where it is at a temperature that is 234 K too low and a  $t_X^2$  that is 0.0089 too high, compared to the true values.

Finally, we comment on Case I. When there is a distinct solution, there may still be errors in the deduced  $T_X$  and  $t_X^2$  resulting from omitting higher-order terms than second order. However, errors are expected to be smaller than for Cases II or III, because Case I is inherently the regime in which there are relatively smaller temperature fluctuations.

### 3.1.2. Application to the Orion Data

Some indication of  $N_e$  in the  $N^+$  zone might be obtained from the  $N_e$  derived from the [S II] lines 6718 and 6733 Å. As is well known, the ratio of these lines has a very weak dependence on  $T_e$ , but we use  $T_e$  that we find later, and find  $N_e = 10275 \text{ cm}^{-3}$ . Unfortunately, our FOS measurements cannot resolve the individual components of [O II] 3727, 3730 (combined, referred to as 3728). It would be very useful to have these measurements for FOS-1SW, because the  $N_e$  in the  $O^+$  region is likely a much better measure of  $N_e$  in the  $N^+$  zone than is the sulfur value.

When we attempt to solve equations (3), (6), and (7) with  $N_e$  from the [S II] lines using the three N II extinction-corrected flux ratios (Table 1), there are no solutions. The behavior is like the test Case II, with the curves even further apart. By ignoring temperature variations ( $t_X^2 = 0$ ), from  $F_{2142}/F_{5756}$ , we find  $T_{65} = 10,884$  K; from  $F_{5756}/F_{6585}$ ,  $T_{54} = 9766$  K; and from  $F_{2142}/F_{6585}$ ,  $T_{64} = 10,263$  K.

Let us now try another value for  $N_e$  and repeat the analysis. In Figure 4a we show the loci for an assumed  $N_e = 6700 \text{ cm}^{-3}$ . The reason for choosing this particular value will become clear in § 3.2.1. The solution at the intersection of the lines for equations (3), (6), and (7) is  $T_X = 9489$  K,  $t_X^2 = 0.0317$ .<sup>13</sup> As for test Case I, there is also a second nonphysical, spurious solution.

Our  $T_X, t_X^2$  solution, graphically portrayed in Figure 4a, is based on actual data. Thus uncertainty in our *HST* line fluxes, relative extinction corrections between these lines, as well as uncertainty in the atomic data used, all contribute to the uncertainty in our inferred values. Suppose, for example, that the observed flux of the 2142 Å lines were lower than measured. That would move the solid and light-dashed curves downward in Figure 4a, lowering the derived  $t_X^2$  and raising the derived  $T_X$  from the intersection, while also

<sup>13</sup> By ignoring temperature fluctuations, one would derive considerably higher electron temperatures:  $T_{65} = 10,623$  K,  $T_{54} = 10,160$  K, and  $T_{64} = 10,370$  K.

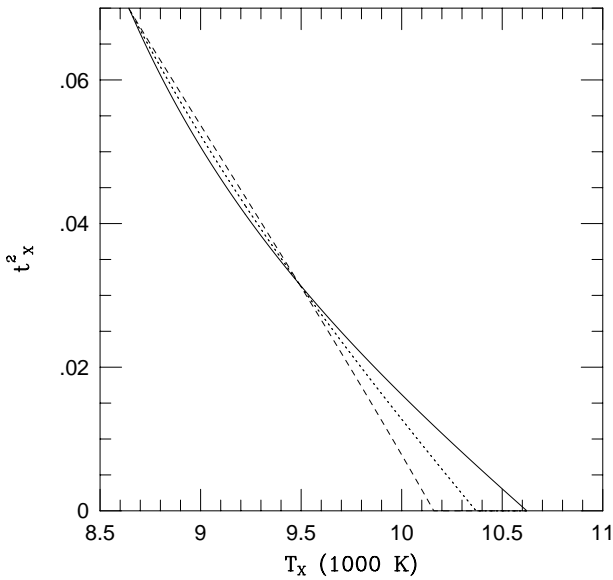


FIG. 4a

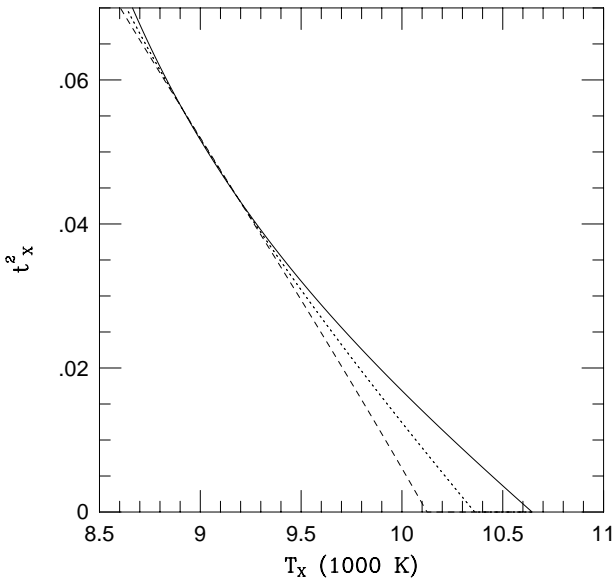


FIG. 4b

FIG. 4.—As Fig. 3, but with Orion extinction-corrected flux ratios in Table 1. (a)  $N_e = 6700 \text{ cm}^{-3}$  is used. The intersection of the loci at  $T_x = 9489 \text{ K}$ ,  $t_x^2 = 0.031655$  is the desired solution. There is also a spurious solution at lower  $T_x$  and higher  $t_x^2$  (see text). (b)  $N_e = 7000 \text{ cm}^{-3}$  is used. This is in the “transition” regime. The intersection of the loci at  $T_x = 9185 \text{ K}$ ,  $t_x^2 = 0.043667$  is the solution.

lowering the values  $T_{65}$  and  $T_{64}$  at the x-intercepts. Clearly, if the measured flux of the 2142 Å line were lowered sufficiently, a situation would be reached (for these atomic data) in which  $T_{65} < T_{54}$ , and no physical solution would be possible. None of the above uncertainties affect the numerical tests in which we generate simulated observations and then use these to infer  $T_x$ ,  $t_x^2$  by the empirical technique. Even though the atomic parameters may be wrong, as long as the same set is used in generating the simulated observables that is used in deriving the empirical equations, it is immaterial to the test results.

The largest value of  $N_e$  that permits a solution for the Orion data is  $7000 \text{ cm}^{-3}$  (to the nearest 100). ( $N_e = 7100 \text{ cm}^{-3}$  renders no intersection.) In Figure 4b, we show this

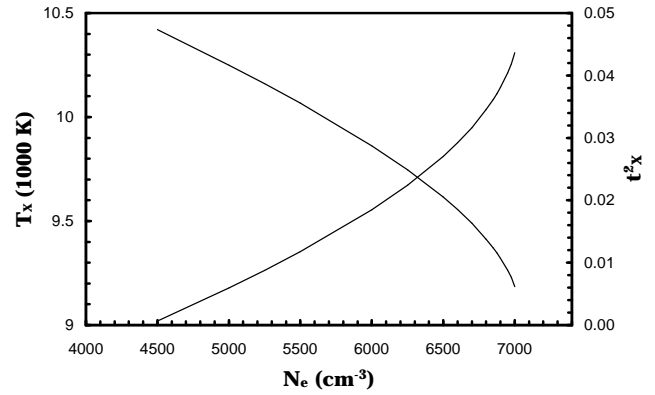


FIG. 5.—With the solution for equations (3), (6), and (7) depending on the assumed  $N_e$ , we calculate a set of “intersection points” (such as in Figs. 3 and 4) for a number of different assumed  $N_e$  values for the Orion ( $\text{N}^+$ ,  $\text{O}^+$ ) region spanning the range in which there are solutions. The line decreasing with increasing  $N_e$  is for  $T_x$ ; the other line is for  $t_x^2$  vs.  $N_e$ .

result, which, as expected, is reminiscent of test Case III. The curves intersect at  $T_x = 9185 \text{ K}$ ,  $t_x^2 = 0.0437$ . With the solution depending on the assumed  $N_e$ , we calculate, where possible, a set of “intersection solutions” for a number of different assumed  $N_e$  values, spanning a reasonable range that may apply to the Orion ( $\text{N}^+$ ,  $\text{O}^+$ ) region. This is shown in Figure 5. Qualitatively, the direction of change can be understood from equations (3), (6), and (7) using the approximations in equations (8), (9), and (10). A decrease in  $N_e$  is also a decrease in  $x$ , causing an increase in the  $F_{2142}/F_{5756}$  ratio and a decrease in both the  $F_{5756}/F_{6585}$  and the  $F_{2142}/F_{6585}$  ratios. These changes cause the equation (3) locus to shift downward and the equation (6) and (7) loci to shift upward (roughly parallel), resulting in the intersection sliding to a higher  $T_x$  and a lower  $t_x^2$  with decreasing  $N_e$ .

There is an additional complication when  $N_e \lesssim 4400 \text{ cm}^{-3}$ . As seen from Figure 5,  $t_x^2$  may reach zero, but cannot go lower. When we attempt to solve equations (3), (6), and (7) with  $N_e \lesssim 4400 \text{ cm}^{-3}$ , then the intercepts  $T_{65} < T_{64} < T_{54}$ , and there is no physically meaningful solution. (There is again the spurious, nonphysical solution at very high  $t_x^2$ ). Indeed, the intercepts  $T_{65} \geq T_{64} \geq T_{54}$ , must hold if there is to be a possible physically meaningful solution. Errors in the measurements or extinction corrections may contribute to where the onset of this low- $N_e$  realm of no solutions occurs. However, in the absence of the above sort of errors, this behavior (no solution when  $N_e$  is below some threshold) is directly related to the  $\text{N}^+$  atomic data adopted, particularly the collision strengths.

### 3.2. Nitrogen to Oxygen Ratio

We continue now with our empirical method analysis to infer N/O values from our *HST* data. The ion ratio by number of  $\text{N}^{+i}/\text{O}^{+i}$ , where  $i$  is the degree of ionization, may be written (see Rubin et al. 1994; Simpson et al. 1995) as

$$\frac{\text{N}^{+i}}{\text{O}^{+i}} = \frac{F_\lambda(\text{N}^{+i})/\epsilon_\lambda(\text{N}^{+i})}{F_\lambda(\text{O}^{+i})/\epsilon_\lambda(\text{O}^{+i})} = \frac{\langle \text{N}^{+i} \rangle \text{N}}{\langle \text{O}^{+i} \rangle \text{O}}. \quad (14)$$

The fractional ionization for element E in ion state  $i$  is defined as

$$\langle \text{E}^{+i} \rangle = \frac{\int N_e N(\text{E}^{+i}) dV}{\int N_e N(\text{E}) dV}. \quad (15)$$

We refer to the value obtained for  $\text{N}^+/\text{O}^+$  from the “traditional” method that uses line fluxes from 6585 and

3728 Å as  $(N^+/O^+)_{\text{opt}}$ .  $T_X$  and  $t_X^2$  can be different for the  $O^+$  region and the  $N^+$  region ( $X$  was used to denote the possibility of different ions).  $N(O^+)$  would replace  $N(N^+)$  in equations (1) and (2). While detailed photoionization models can produce theoretical values for  $T_X$  and  $t_X^2$  in both  $N(O^+)$  and  $N(N^+)$ , among others, with the empirical analysis there is no means of distinguishing possible different values. Hence, we assume that  $T_X$  and  $t_X^2$  found for  $N^+$  apply for both zones. Unless the ionization structure is the same for both, this assumption may not be correct.

The evaluation of  $(N^+/O^+)_{\text{opt}}$  from equation (14) with the additional  $C_{\text{ivar}}$  factor from equation (4) is accomplished by solving the five- or six-level atom for the populations apropos to the  $N_e$ ,  $T_e$  values. This provides the necessary values for  $\epsilon_\lambda$ . As was done earlier, we “factor out” the differential Boltzmann factor dependence and write

$$\left(\frac{N^+}{O^+}\right)_{\text{opt}} = \frac{K'_{23}}{K_4} \exp\left(-\frac{16548}{T_X}\right) \frac{F_{6585}}{F_{3728}} \frac{1 + b_{3728} t_X^2}{1 + b_{6585} t_X^2}. \quad (16)$$

In this equation,  $(K'_{23}/K_4) \exp(-16548/T_X) = (\epsilon_{3727} + \epsilon_{3730})/\epsilon_{6585}$ ;  $K_4$  refers to level 4 of  $N^+$  as before, and  $K'_{23}$  refers to levels 2 and 3 of  $O^+$ .

As in equations (8)–(10), it is sometimes useful to approximate the ratio of  $K$ s for low density:  $K'_{23}/K_4 \sim 2.456/(1 + 1.200x)$ . Because at least one of the two components comprising 3728 (blended here) suffers collisional deexcitation at the  $N_e$  values expected for Orion, additional terms in this simple approximation would be needed to try to account for differential collisional deexcitation of 3727 and 3730. Our purpose in mentioning this at all is for its limited application as long as none of the pertinent lines undergoes significant collisional deexcitation. Again, we deal directly with the  $\epsilon$  values throughout.

Let us now write the analogous relation for  $(N^+/O^+)_{\text{uv}}$  using  $N \text{ II}]$  2142 and  $[O \text{ II}]$  2471:

$$\left(\frac{N^+}{O^+}\right)_{\text{uv}} = \frac{K'_{45}}{K_6} \exp\left(+\frac{9089}{T_X}\right) \frac{F_{2142}}{F_{2471}} \frac{1 + b_{2471} t_X^2}{1 + b_{2142} t_X^2}. \quad (17)$$

A low-density approximation may be written as  $K'_{45}/K_6 \sim 0.1512(1 + 2.667x)$ .<sup>14</sup>

To check the validity of using equations (16) and (17) to estimate  $N^+/O^+$ , we continue with the test cases used in § 3.1. In addition to the earlier mentioned generated “observables,” we now also use the  $F_{3728}$  and  $F_{2471}$  fluxes in equations (16) and (17) as if they were real observations. These are solved using the values found in § 3.1 for  $T_X$  and  $t_X^2$ , and compared with the input  $N^+/O^+$ , arbitrarily set to unity for simplicity.

For Case I, equations (16) and (17) provide excellent agreement (to better than 0.9%) with the input value if we use either the analytical ( $T_X = 9500$  K,  $t_X^2 = 0.033241$ ) or the inferred intersection solution (9446 K, 0.034121). With these

<sup>14</sup> Even though the 2471 Å lines (from levels 4 and 5) have high  $N_{\text{crit}}$ , their volume emissivities become affected at the lower  $N_{\text{crit}}$  of the 3730 Å (lowest) and 3727 Å lines (from levels 2 and 3), because then, the level 2 and 3 populations start to “saturate” at Boltzmann values; consequently, excitations from levels 2, 3 to 4, 5 become important, increasing the 2471 emissivities above that produced by excitations from the ground state alone. At the same time, the volume emissivity of the 3728 lines saturates (the normalized volume emissivity starts decreasing). Hence the range of usefulness of this approximation is also set by the lowest  $N_{\text{crit}}$ , that of the 3730 line.

values for temperature and no correction for  $T_e$  fluctuations,  $(N^+/O^+)_{\text{opt}}$  is 10%–11% too low, while  $(N^+/O^+)_{\text{uv}}$  is 12%–13% too high. For Case II (no solution), when we use the analytical ( $T_X = 8000$  K,  $t_X^2 = 0.046875$ ), equations (16) and (17) provide values that are slightly larger than input but within 1.4%. If no correction is made for  $T_e$  fluctuations,  $(N^+/O^+)_{\text{opt}}$  is  $\sim 21\%$  too low and  $(N^+/O^+)_{\text{uv}}$  is  $\sim 21\%$  too high. For Case III (“transition” solution), when we use either the analytical ( $T_X = 9000$  K,  $t_X^2 = 0.037037$ ), or the inferred intersection solution (8766 K, 0.045909), the equations provide values that are within 1.4% of the input quantity. If we use  $T_X = 9000$  K with no correction for  $t_X^2$ , then  $(N^+/O^+)_{\text{opt}}$  is  $\sim 13\%$  too small, while  $(N^+/O^+)_{\text{uv}}$  is  $\sim 15\%$  too high. The corresponding abundance ratios with  $T_X = 8766$  K are  $\sim 19\%$  too small and  $\sim 18\%$  too high. The bottom line from these tests is that it is important to correct for  $T_e$  variations in deriving  $N^+/O^+$ . For this purpose the inclusion of the  $t_X^2$  terms is sufficient.

### 3.2.1. Applications to the Orion Nebula Data

From our derivation of the shape of the Orion extinction curve (Martin et al. 1998), the effect of differential extinction is larger in the case of the optical derivation of  $N^+/O^+$  than in the case of the UV determination, and in the opposite direction. For FOS-1SW we find that the observed ratio  $F_{2142}/F_{2471}$  must be increased by a factor of 1.32, which is less than the correction for  $F_{6585}/F_{3728}$ , which requires a decrease by a factor of 1.70.

Let us now use the various values considered for  $N_e$  for the  $(N^+, O^+)$  zone, using the set of solutions displayed in Figure 5. We apply the analysis of § 3.2 using the extinction-corrected flux ratios to derive  $(N^+/O^+)_{\text{opt}}$  from equation (16) and  $(N^+/O^+)_{\text{uv}}$  from equation (17). The resulting loci for each determination are shown in Figure 6. These end at  $N_e = 7000 \text{ cm}^{-3}$ , the largest value of  $N_e$  that permits a solution for the Orion data. Fortuitously, the two curves just cross at approximately this density. It is reasonable to consider this a “preferred” solution, because

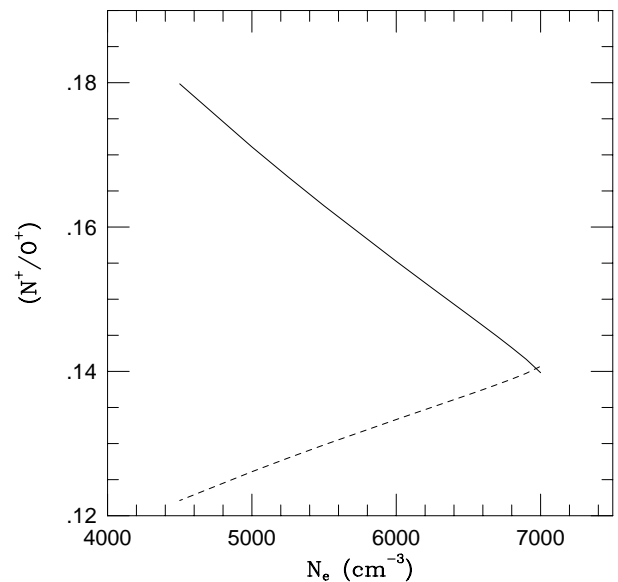


FIG. 6.—Resulting loci for the determination of  $(N^+/O^+)_{\text{opt}}$  (solid line) and  $(N^+/O^+)_{\text{uv}}$  (dashed line) vs.  $N_e$  when we use the set of solutions shown in Fig. 5. The two curves intersect at a point, which we consider our “preferred” solution  $N^+/O^+ = 0.14$ , because the two methods should provide similar results.

the two methods should provide similar results. Here, using  $T_X = 9185$  K,  $t_X^2 = 0.0437$ ,  $(N^+/O^+)_{\text{opt}} = 0.1222(1.144) = 0.1398$  and  $(N^+/O^+)_{\text{uv}} = 0.1626(0.8651) = 0.1407$ . The quantities in parentheses are the respective correction factors ( $C_{\text{ivar}}$ ) due to  $t_X^2$  terms. We shall need to revisit these values later. The lack of solutions when  $N_e > 7000$  for Orion is presumably due to the inadequacy of the  $t_X^2$  representation when  $T_e$  variations are large. Nevertheless, the trend of  $(N^+/O^+)_{\text{opt}}$  decreasing and  $(N^+/O^+)_{\text{uv}}$  increasing with increasing  $N_e > 7000$  is expected to continue. Thus, where the two determinations are equal is unique and well defined.

We see that the  $N^+/O^+$  values depend on  $T_e$  differently, with  $(N^+/O^+)_{\text{uv}}$  being the less sensitive and in the opposite direction from  $(N^+/O^+)_{\text{opt}}$ . It is interesting (and perhaps counterintuitive) that the derived value  $(N^+/O^+)_{\text{uv}}$ , depending on the circumstances, may (the case for the Orion analysis plotted here) or may not be actually *more* sensitive to  $t_X^2$  than is  $(N^+/O^+)_{\text{opt}}$ . Some indication of the sensitivity of the  $N^+/O^+$  inferred may be obtained by continuing with the example used in § 3.1.2. Again, suppose the observed flux of the 2142 Å lines were lower than measured: for a fixed  $N_e$ , this causes the derived  $T_X$  to be higher and  $t_X^2$  lower. As a result of higher  $T_X$ ,  $(N^+/O^+)_{\text{opt}}$  would be larger, and  $(N^+/O^+)_{\text{uv}}$  would be smaller. However, as a result of lower  $t_X^2$ ,  $(N^+/O^+)_{\text{opt}}$  would be smaller and  $(N^+/O^+)_{\text{uv}}$  larger. Furthermore,  $(N^+/O^+)_{\text{uv}}$  would be smaller in direct proportion to the lower measured 2142 Å flux. The upshot of these competing effects is to make little change in the derived  $N^+/O^+$ ; for our preferred Orion solution, lowering the measured 2142 Å flux by a factor of 1.1 raises  $(N^+/O^+)_{\text{opt}}$  by a factor 1.015 and lowers  $(N^+/O^+)_{\text{uv}}$  by a factor 1.034.

In view of the results encountered with the linear test cases, we feel that some adjustment is necessary to the  $(T_X, t_X^2)$  solution near the high- $N_e$  end of the curves in Figure 5. As the “transition” value of  $N_e = 7000 \text{ cm}^{-3}$  is approached, both  $T_X$  and  $t_X^2$  are changing rather dramatically; When  $N_e$  changes from 6800 to 7000  $\text{cm}^{-3}$ ,  $T_X$  changes from 9413 to 9185 K, and  $t_X^2$  changes from 0.03453 to 0.04367. We may draw on the results of the linear test cases for guidance. Case III (Fig. 3c) was also for a “transition” regime (from solution to no solution). There, predominantly as a result of not accounting for  $t_X^4$  terms, the solution of equations (3), (6), and (7) was found to be at a temperature that was 234 K too low and a  $t_X^2$  that was 0.0089 too high, compared to the true values. The indication from further test cases at  $N_e = 7000 \text{ cm}^{-3}$  (close to the value we find for Orion) is that the necessary adjustment will be even larger. We use the linear test case that has been fine-tuned to match the Orion results as our best means of adjustment (see Appendix B). For this,  $T_X$  is 337 K too small and  $t_X^2$  is 0.01217 too large, compared to the true values. We apply these differences to the Orion “solution” at  $N_e = 7000$  to arrive at the preferred values  $T_X = 9522$  K and  $t_X^2 = 0.0315$  (which happens to be close to what we find for  $N_e = 6700 \text{ cm}^{-3}$ : 9489 K and 0.0317; see Fig. 4a).

As for our best estimate  $N^+/O^+ = 0.14$ , this is affected little by the fact that the  $O^+$  lines suffer collisional deexcitation when  $N_e \sim 7000 \text{ cm}^{-3}$ . The “tailor-made” Orion test case in Appendix B indicates that our inferred  $(N^+/O^+)_{\text{opt}}$  and  $(N^+/O^+)_{\text{uv}}$  values need to be adjusted by only small factors: an increase of 1.031 and a decrease of 1.037, respectively. Revisiting a calculation made earlier in this sub-

section and adjusting for these factors, we find what are deemed our best estimates:  $(N^+/O^+)_{\text{opt}} = 0.1442$  and  $(N^+/O^+)_{\text{uv}} = 0.1357$ . When we calculate these ratios directly from equations (16) and (17) using the corrected  $T_X = 9522$  K,  $t_X^2 = 0.0315$ ,  $(N^+/O^+)_{\text{opt}} = 0.1432$  and  $(N^+/O^+)_{\text{uv}} = 0.1396$ . These are, respectively, factors of 1.007 too small and 1.029 too large, compared to the correct values (as determined from the tailor-made test case).

It is important to realize that in general  $N/O \neq N^+/O^+$ . With the empirical approach, the way to convert  $N^+/O^+$  to  $N/O$  is with the ratio of fractional ionizations using the right-hand side of equation (14). This is identical to applying ionization correction factors (*icfs*; see e.g., Rubin et al. 1994; Simpson et al. 1995). Unless the ionization structure of  $N^+$  and  $O^+$  is the same, this is necessary. The assumption is often made that the  $N^+$  and  $O^+$  zones are coextensive and that  $N/O \sim N^+/O^+$ . For a number of models typifying parameter space for Galactic H II regions (e.g., Rubin 1985),  $N/O$  significantly exceeds  $N^+/O^+$ , while the opposite is not true. Recent work by Stasinska & Schaerer (1997) that computed nebular models based on new non-LTE (NLTE) stellar atmospheres finds that  $N/O \sim N^+/O^+$  over the range of interest for H II regions. They attribute this to the flatter ionizing spectrum of the new NLTE stellar atmosphere models compared to the earlier LTE model atmospheres used by Rubin (1985). We shall return to this later.

#### 4. INTERPRETATION WITH PHOTOIONIZATION MODELS

This technique has certain advantages over the empirical method. We mention a few that may be important for the purpose of deriving reliable  $N/O$  abundances from the data. Perhaps most important is the self-consistent calculation of the  $T_e$  and ionization structure. The model then naturally supersedes having to specify explicitly average temperatures and  $t^2$  (and if desired, even higher-order quantifiers of temperature variations) for the ionic species treated. It is also unnecessary to make ad hoc applications of *icfs*.

Another advantage is the ability to simulate physical processes that involve different ionic states as they affect the equilibrium level populations. For instance, recombinations and charge transfer reactions may provide significant routes into the energy levels of species  $X^i$  that are not negligible compared to collisional processes. Accounting for these “recombination”-type processes requires knowledge of the structure/properties of the next higher ionic state  $X^{i+1}$ . There can also be situations in which it is necessary to know the structure/properties of the next lower ionic state  $X^{i-1}$ . For example, there may be significant routes into the energy levels of species  $X^i$  via photoionizations to excited states (“photoionization excitation”; e.g., Rubin 1986; Petuchowski & Bennett 1995).

Of course, the theoretical modeling approach has its limitations. One does not know completely the three-dimensional  $T_e$ ,  $N_e$ , and density structure of all ionic species. Indeed, the input density distribution and geometry require a huge compromise with true nebular reality. Use of the empirical methods in this paper provides a complementary check on whether the assumed density distribution/geometry is reasonable, and whether some treatment of the physics is missing or too approximate to simulate reality.

##### 4.1. Photoionization Modeling Treatment

Since the work of Zuckerman (1973) and Balick, Gammon, & Hjellming (1974), it has been realized that the

overall spatio-kinematic picture presented by the Orion Nebula data is that of a “blister” configuration. The Trapezium stars and the ionized gas lie in the foreground of the molecular cloud OMC 1—all of which are viewed roughly face-on. Before acquiring these *HST* data, detailed photoionization modeling with such a blister geometry had been applied to Orion data in order to understand its structure and properties (Baldwin et al. 1991; Rubin et al. 1991a). We now take these two independent, previously proposed Orion models (of different regions in the nebula) and apply them to make predictions of the flux expected for N II] 2142 Å and the other lines relevant to this paper. Some adjustments to these earlier models have been made to include in each code the same updated treatment for the statistical equilibrium of the populations of the N and O ions discussed here. We use the *same* collision strengths and *A*-values as for the empirical derivations (see Appendix A).

Besides collisional excitation/deexcitation and spontaneous emission, there are additional mechanisms that may influence the N<sup>+</sup> six-level populations. For both codes we include terms for an effective recombination rate into levels 4 and 5.<sup>15</sup> This consists of two contributions—an effective radiative recombination coefficient using the  $T_e$ -dependent expression from Péquignot, Petitjean, & Boisson (1991) and an effective dielectronic recombination coefficient using the  $T_e$ -dependent expression from Nussbaumer & Storey (1984). These rates depend on the number of N<sup>++</sup> ions recombining, and hence on the details of the modeling ionization equilibrium calculations, something that is not treated with the empirical procedure. We note that for both <sup>1</sup>D<sub>2</sub> and <sup>1</sup>S<sub>0</sub>, the effective radiative coefficient is much larger than the effective dielectronic coefficient. The inclusion of these “recombination” routes obviously has the largest effect on the equilibrium level populations when N<sup>+++</sup> ≫ N<sup>+</sup>.

Nahar calculated total recombination coefficients in a unified fashion without separating radiative from dielectronic coefficients. The latest table (an Erratum) providing these for certain  $T_e$  values includes recombinations to N<sup>+</sup> (Nahar 1996). At  $T_e = 10^4$  K, this value is  $3.08 \times 10^{-12} \text{ cm}^3 \text{ s}^{-1}$ , which is lower than the total  $4.39 \times 10^{-12} \text{ cm}^3 \text{ s}^{-1}$  arrived at by summing the radiative (2.35; Péquignot et al. 1991) and dielectronic (2.04; Nussbaumer & Storey 1983) coefficients.

There is also a route to populating some of the levels via the charge transfer reaction N<sup>+++</sup> + He<sup>0</sup> → N<sup>+</sup> + He<sup>+</sup>. Sun et al. (1996) provide the total rate coefficient as well as an effective rate coefficient into <sup>3</sup>P and <sup>1</sup>D<sub>2</sub>. A laboratory measurement of the total rate coefficient is  $8.67 \pm 0.76 \times 10^{-11} \text{ cm}^3 \text{ s}^{-1}$  at 3900 K (Fang & Kwong 1997). This agrees with the Sun et al. (1996) rate coefficient within the 1  $\sigma$  uncertainty. We include the contribution into <sup>1</sup>D<sub>2</sub>; this could influence the calculation only when N<sup>+++</sup> ≫ N<sup>+</sup>. Under most practical circumstances, this effect should prove negligible.

In this paper we are not constructing a new model. That is one of our goals for future interpretation of our *HST* data

set as well as other observations with a new generation of non-LTE model atmospheres and other improvements since our earlier (1991) models. We now maintain the original density/geometry of those models, but in order to narrow the differences in input parameters, we arbitrarily use the Rubin et al. ionizing spectrum and abundance set and no grains. We have also now modified the individual codes to treat the calculation of the N<sup>+</sup> and O<sup>+</sup> level populations the same, as described above. We continue with the separate codes to perform the ionization and thermal equilibria calculations independently. This in itself will cause differences in our predicted line fluxes.

The procedure used here to address the N/O ratio with the separate models is as follows. We compute models with the elemental abundance set used by Rubin et al. (1991a, b). From these models we obtain predicted surface brightnesses for the various emission lines. For NEBULA we use surface brightnesses for a column offset from the model center that correspond with the 32" that 1SW is from  $\theta^1$  Ori C. The CLOUDY model is of a region 40" west of  $\theta^1$  Ori C. For our separate models we then prorate input nitrogen abundance to force the predicted line ratio to match the extinction-corrected observed N II] 2142/[O II] 2471 ratio, yielding (N/O)<sub>uv</sub>. The same is done for the [N II] 6585/[O II] 3728 ratio, which provides (N/O)<sub>opt</sub> and the observed [N III] 57  $\mu$ m/[O III] 52  $\mu$ m ratio, yielding (N/O)<sub>ir</sub>. For the (N/O)<sub>ir</sub> determinations, we match to  $F_{5.7}/F_{5.2} = 0.13$  (Rubin et al. 1991a) at a position that might be typical for our *HST* locations. These N/O ratios are assumed to be our final values here.

The retrofit of the Baldwin et al. (1991) model gives (N/O)<sub>uv</sub> = 0.178, (N/O)<sub>opt</sub> = 0.133, and (N/O)<sub>ir</sub> = 0.178, while the retrofit of the Rubin et al. (1991a) model gives respectively, 0.171, 0.155, and 0.174. We do not seek further refinement by rerunning our models with any of these other nitrogen abundances. Strictly speaking, the proration process is not entirely valid, because a change in the N abundance will somewhat modify the structure (most directly the temperatures via its cooling lines). Because oxygen is the dominant coolant, we chose not to alter its input abundance, which would bring about major changes to the models. For the purpose of determining the relative differences in the inferred N/O values from the three different wavelength regions and two separate models, the procedure used is sufficient. According to these models, there is no significant contribution to the N<sup>+</sup> or O<sup>+</sup> line emission from the noncollisional routes to populating the pertinent energy levels. Thus, the empirical treatment presented should not suffer on that score.

## 5. DISCUSSION AND CONCLUSIONS

We highlight and discuss the main points of the paper.

1. *HST* measurement of the N II] 2140, 2143 Å lines in the Orion Nebula permits several new astrophysical applications. In conjunction with *HST* line measurements of [N II] 5756 and 6585 Å in the same aperture/location, we are able to address the average electron temperature and  $t^2$  in the particular observed N<sup>+</sup> volume with an empirical method.

2. When we utilize the fluxes of the nitrogen lines above with our cospatial measurements of the [O II] 2471 and 3728 Å lines, we are able to derive the N<sup>+</sup>/O<sup>+</sup> ratio empirically in two ways. We determine (N<sup>+</sup>/O<sup>+</sup>)<sub>uv</sub> from the N II]

<sup>15</sup> There is no contribution to level 6, because under the assumption of LS coupling, recombinations from the N<sup>+++</sup> ground state <sup>2</sup>P<sup>0</sup> cannot result in quintet states of N<sup>+</sup>. Nussbaumer & Storey (1984) discuss implications of relaxing LS coupling. We neglect recombinations to the <sup>3</sup>P<sup>1,2</sup> levels (2 and 3) in solving for the level populations, because the contribution is dwarfed by collisional excitation.

2142/[O II] 2471 ratio and  $(N^+/O^+)_{\text{opt}}$  from the well-known [N II] 6585/[O II] 3728 ratio. Each of these abundance ratios is formulated in terms of the average  $T_e$  and  $t^2$ . Our preferred empirical solution is obtained by requiring that  $(N^+/O^+)_{\text{opt}}$  and  $(N^+/O^+)_{\text{uv}}$  be equal. This yields, for the  $(N^+, O^+)$  zone, an average electron density of  $\sim 7000 \text{ cm}^{-3}$ , an average  $T_e = 9500 \text{ K}$ ,  $t^2 = 0.032$ , and  $N^+/O^+ = 0.14$ . The reliability of the empirical analysis for  $N^+/O^+$  is dependent on how closely the  $N^+$  and  $O^+$  volumes coincide, in order that the average  $T_e$  and  $t^2$  for the  $N^+$  region also be valid for the  $O^+$  region. Walter & Dufour (1998) have summarized published results of  $t^2$  in Orion covering the past 30 years. Values in the literature range from a low of  $\leq 0.015$  (Shaver et al. 1983) to a high in excess of 0.1 (Peimbert & Costero 1969), with most values in the range of 0.03–0.04. Therefore, the result of 0.032 from this study is typical of the values found by others. We think that detailed comparisons with results published by others is not warranted here, given different observational lines-of-sight/apertures, data sets, analysis techniques, extinction-correction methods, atomic data utilized, etc. If one were to try such an exercise, we would suggest beginning with the observations and applying, as homogeneously as possible, items in the above-mentioned list—particularly the atomic data set (which, in principle, should always be feasible).

3. If  $t_X^2 \gtrsim 0.04$ , then the method to derive  $T_X$  and  $t_X^2$  from the  $N^+$  lines may start to suffer from the omission of higher-order  $T_e$ -variation terms. This could be manifested by an inability to find a solution (common or any) to the set of three  $N^+$  flux ratio equations. Even if there is a solution that finds such a high  $t_X^2$ , one needs to be cognizant of the possibility that the solution is somewhat in error because of the omission in the analysis of higher-order terms that are no longer negligible. We demonstrated the above with test cases using a linear  $T_e$  variation;  $t_X^4$  terms were identified as the source of disparity ( $t_X^3 = 0$ ). In general,  $t_X^3$  terms will not be zero. However, because positive and negative contributions to the sum (integral) will offset each other,  $|t_X^3|$  should be significantly smaller than  $t_X^4$ . Thus, it is likely that the  $t_X^4$  terms will be the next most important in the Taylor series treatment after the  $t_X^2$  terms.

4. We also derive  $(N/O)_{\text{uv}}$ ,  $(N/O)_{\text{opt}}$ , and  $(N/O)_{\text{ir}}$ , using our two previous photoionization models of Orion. This is done by prorating the input N/H ratio (while maintaining the O/H ratio) to obtain agreement between the respective extinction-corrected line fluxes and the model predictions for these same flux ratios. There is fair agreement, with all the values derived from the two models falling in the range from 0.133 to 0.178. To compare the photoionization modeling results with the empirically derived  $N^+/O^+$  value requires a correction for the possibility that the  $N^+$  and  $O^+$  regions are not identical. Such a correction is equivalent to applying *icfs*, which often are inferred using photoionization models as guides. Our current models have  $\langle N^+ \rangle / \langle O^+ \rangle$  less than unity. However, the recent grid of nebular models by Stasinska & Schaerer (1997) based on new NLTE stellar model atmospheres finds that  $N/O \sim N^+/O^+$  over the range of interest for H II regions. We are continuing work toward producing a significantly improved Orion Nebula model. Our plans are to include a more realistic representation of the ionizing spectrum using new NLTE stellar model atmospheres. At present, our overall assessment of the gas-phase N/O ratio is that it is in the range of  $\sim 0.13$ – $\sim 0.18$ .

5. It appears from the present analysis that there is reasonable agreement between  $(N/O)_{\text{ir}}$  and the other two determinations,  $(N/O)_{\text{opt}}$  and  $(N/O)_{\text{uv}}$ . We note that the current range determined for N/O is somewhat higher than  $(N/O)_{\odot} = 0.126$  (Grevesse & Noels 1993). Our mean value of  $N/O = 0.16 \pm 0.03$  in Orion is considerably higher than the mean value (0.034) found in irregular galaxies (Vila-Costas & Edmunds 1993), indicating that approximately 75% of the nitrogen in the solar neighborhood is due to secondary nucleosynthesis. As noted previously, this N/O ratio is slightly higher than found for the Sun, which would be expected, given that the Sun is  $\sim 5 \text{ Gyr}$  old. However, there remains the question of the O/H value in Orion compared to solar. Recent studies (Meyer et al. 1994; Mathis 1995; based on ISM absorption-line and theoretical nebular model analyses, respectively) have indicated that O/H in Orion is probably *lower* than determined for the Sun. While this would be odd from the point of view of homogeneous evolution of the Galactic abundances near the solar circle, it would tend to reinforce our higher-than-solar N/O ratio for Orion. Note that most previous studies have, by contrast, found lower N/O ratios, based on the  $N^+/O^+ 6585/3728$  line ratios.

6. It is important to use the *same* atomic data set when using and comparing results from photoionization models and empirical methods.

7. The FOS flux ratio of N II] 2142/[O II] 2471 is a factor of  $\sim 1.6$  higher than the GHRS ratio. The GHRS aperture is a factor of 5.2 larger in area than the FOS aperture. The FOS  $F_{2471}$  is  $\sim 1.18$  times higher than its average flux value over the circumscribed GHRS aperture (see surface brightnesses in Table 1). This seems to imply that FOS is seeing a N II] bright spot with things varying on a small scale. We have examined the digital forms of the WFPC2 imagery (O'Dell collection) and our WFPC2 H $\beta$  data. The H $\alpha$  and H $\beta$  data have been combined to produce a  $C(\text{H}\beta)$  map.  $C(\text{H}\beta)$  is the  $\log_{10}$  extinction-correction factor at H $\beta$  and is determined to be 0.605 for FOS-1SW. We have also examined a three-color image ([O III] 5008, H $\alpha$ , and [N II] 6585). For a  $3'' \times 3''$  region around 1SW,  $C(\text{H}\beta)$  varies by less than  $\pm 0.04$ , which results in no more than a  $\pm 2\%$  change in the 2142/2471 flux ratio due to differential extinction (Martin et al. 1998). The [N II]/H $\alpha$  ratio varies by no more than 10%. Over an area 1'.98 square centered on 1SW, the minimum and maximum pixel-pixel variation (400 pixels 0'.0991 square) in [N II] 6585 observed surface brightness are  $1.320 \times 10^{10}$  and  $2.525 \times 10^{10} \text{ photons cm}^{-2} \text{ s}^{-1} \text{ sr}^{-1}$ , an extreme variation of a factor of 1.91. Our general impression is that over an area  $\sim 5''$  square centered on 1SW, the region is quite smooth in all of the WFPC2 imaged lines and continuum. No subarcsecond knots are evident. Therefore, we surmise that the measured differences in the flux ratio of N II] 2142/[O II] 2471 are due, at least in part, to the accuracy of the absolute calibration of FOS and GHRS (which is further complicated because Orion is an extended source).

8. Our plans for Cycle 7 with STIS include a slit spectrum through position 1SW. This should resolve individually [O II] 3727, 3730 Å, providing needed  $N_e$  information. Our FOS 3728 measurement presented here also suffers from blending by other emission lines, which STIS data should help decipher. H13 and H14 ( $\lambda_{\text{vac}}$  at 3735.44 and 3723.01) are certainly “swallowed” in the full width of the observed feature, as is also [S III] 3722.90 Å. We estimate

from our measured fluxes of the adjacent Balmer lines, our extinction factors (Martin et al. 1998), and H-recombination (case B) emissivities for  $T_e = 9000$  K,  $N_e = 5000$  cm $^{-3}$  (based on Storey & Hummer 1995), that the contribution of H13 plus H14 is 3.1%. Our estimate of the contribution to the flux by [S III] 3722.90 is  $\sim 0.8\%$ . This is obtained from our FOS-measured flux ( $1.88 \times 10^{-14}$ ) for [S III] 6314 (same upper level as 3722.9),  $A$ -values compiled by Mendoza (1983), and differential extinction (Martin et al. 1998). The total contamination by these three lines is thus roughly 4%. We have not made any reduction for this to the tabulated flux we are using for [O II]. Our rationale for not doing so here is that the uncertainty is likely greater because of fitting the underlying continuum, which is changing considerably across the 3728 feature. If the [O II] 3728 flux were decreased by 4%, our estimates of both  $(N^+/O^+)_{\text{opt}}$  and  $(N/O)_{\text{opt}}$  would increase slightly.

Our planned STIS program will also observe the O III 1661–1666, 4364, and 5008 Å lines, enabling a similar analysis to be performed to obtain  $T_X$  and  $t_X^2$  in the O $^{++}$  region. We shall also measure the N III 1747–1754 Å lines in order to derive  $N^{++}/O^{++}$ . Now, from our FOS-1SW data, we are able to obtain  $T_e$  in the observed O $^{++}$  region empirically from the extinction-corrected ratio  $F_{4364}/F_{5008} = 0.00424$ . We use the latest version of the “Lick FIVE-LEVEL” atom program (DeRobertis, Dufour, & Hunt 1987), updated for newer atomic data (Shaw & Dufour 1995). For  $N_e = 5000$  and  $10,000$  cm $^{-3}$ ,  $T_e = 8833$  and  $8771$  K. What would be expected in view of our analysis in terms of  $T_X$  and  $t_X^2$  (but for the O $^{++}$  region) is that this is a maximum temperature (with  $t_X^2 = 0$ ). When  $t_X^2 > 0$ ,  $T_X$  will

be smaller. A cospatial observation of O III 1661–1666 should help determine this.

We speculate that the current rather large value derived for  $t^2$  may result from the narrow FOS solid angle (represented by a cylinder cutting through the nebula) experiencing relatively more local “meteorology” (small-scale structure). One might wonder if  $t^2$  inferred for a larger volume would be smaller. Our Cycle 7 long-slit STIS observations should be able to test this. Nevertheless, the explanation of values of  $t^2$  as large as 0.032 remains a challenge for “standard” photoionization models.

9. As stated, we plan to pursue an improved theoretical model for Orion. We also plan further investigation of the empirical methods presented. These include studying the effects of density variations and using other atomic data, such as substituting the Lennon & Burke (1994)  $N^+$  effective collision strengths.

We are grateful to C. R. O’Dell and Abby Wong for assistance on many aspects of this program. We thank Jeff Fuhr, Charlotte Froese-Fischer, and Francis Keenan for providing information and helpful discussions; we thank Christopher Ortiz for help with the computations and both Donald Clayton and Janet Simpson for helpful comments. Support for this work was provided by NASA through grants GO-4385, GO-5748, and GO-6056 from the STScI. R. J. D. and G. J. F. acknowledge NASA/Ames Research Center Interchange grants NCC 2-5199 and NCC2-5193, respectively. R. H. R. acknowledges NASA/Ames Research Center contract NAS2-14218 with Orion Enterprises and thanks Scott McNealy for providing a Sun workstation.

## APPENDIX A

### ATOMIC DATA FOR $N^+$ AND $O^+$

For this paper we adopt the following data sets:

*Collision strengths for  $N^+$ .*—Values for all six lowest-lying levels are from Stafford et al. (1994). We use the effective collision strengths for 10,000 K; these do not vary much with the  $T_e$  range of interest in Orion. There is another contemporaneous calculation by Lennon & Burke (1994) that has somewhat different values. We chose to use the Stafford et al. results because they have included more terms.

*Collision strengths for  $O^+$ .*—Values for the effective collision strengths between the three lowest states are taken from McLaughlin & Bell (1993) for 10,000 K. These vary little with  $T_e$  within the range of interest here. In order to obtain collision strengths between the five lowest-lying levels (including the fine structure), we partitioned by the appropriate statistical weights; however, we scale the Pradhan (1976) individual collision strengths between levels 2–4, 2–5, 3–4, and 3–5 by a factor of 1.207 to adjust the term sum (of these four) to the McLaughlin & Bell value.

*A-values.*—For both  $N^+$  and  $O^+$ , these are taken from Wiese, Fuhr, & Deters (1996). One of the original sources for these data is Froese-Fischer & Saha (1985). There are differences between the values in Wiese et al. (1996) and the original references, because the former used observed wavelengths and/or energy levels and adjusted  $A$ -values to conform to these observed levels. For the crucial N III] 2143.45, 2139.68 Å lines of interest here, there have been laboratory measurements for the  $A$ -values (Calamai & Johnson 1991). We use an updated recommended value of  $A(6-2) = 54.4$  s $^{-1}$  and  $A(6-3) = 125.8$  s $^{-1}$  (J. Fuhr 1997, private communication).

*Energy levels.*—For  $N^+$  and  $O^+$ , these are taken from compilations by Mendoza (1983) or Wiese et al. (1996). From these we obtain the values for  $\chi$ , the excitation energy above the ground state for the upper level of a transition. For  $N^+$ , level 4 ( $^1D_2$ ), level 5 ( $^1S_0$ ), and level 6 ( $^5S_2$ ) are 22035, 47028, and 67312 K above the ground state. Differences between these  $\chi$ s are used in equations (3), (6), and (7), where the exponential term is referred to as the differential Boltzmann factor. For  $O^+$ , levels 2 and 3 ( $^2D_{5/2, 3/2}$ ) and levels 4 and 5 ( $^2P_{3/2, 1/2}$ ) are combined in the empirical treatment. The fine-structure splitting of each of these terms is thus neglected. We weight by the statistical weights of the respective fine-structure levels to obtain  $\chi_{23} = 38583$  and  $\chi_{45} = 58223$  K above the ground state. Differences between these  $\chi$ s and those for  $N^+$  are used in equations (16) and (17).

## APPENDIX B

## ADDITIONAL LINEAR TEST CASES

Here we present the results of additional tests of the empirical procedures utilized in § 3. There we used simple cases having  $T_e$  vary linearly with position and used  $N_e = 1 \text{ cm}^{-3}$ . In order to provide further guidance in assessing the Orion Nebula results, we repeat the same three tests here using  $N_e = 7000 \text{ cm}^{-3}$ , which is close to the value found for our “preferred” solution. The repeat calculation with the Case I (Fig. 3a)  $T_e$  distribution produces no intersection. However, the three loci approach each other (within 1%), making this very close to the “tangent” situation. The closest approach is for  $T_X = 9064 \text{ K}$ ,  $t_X^2 = 0.049786$ . This is 436 K less and 0.016545 greater than the true (analytical) values. The calculation with the Case II (Fig. 3b)  $T_e$  distribution, with  $N_e = 7000 \text{ cm}^{-3}$ , produces no intersection; the three loci are even further apart. For the Case III (Fig. 3c)  $T_e$  distribution, when  $N_e = 7000 \text{ cm}^{-3}$  there is now no solution.

Finally we fine-tune a linear test case in order to replicate the  $(T_X, t_X^2)$  solution that we find for the Orion data when  $N_e = 7000 \text{ cm}^{-3}$ . This is accomplished when  $T_e$  varies linearly from 6596–12450 K and results in  $T_X = 9523 \text{ K}$ ,  $t_X^2 = 0.031490$ , and  $t_X^2 = 0.0017850$ , analytically. (To generate the “observed line fluxes” throughout this paper, we use an integration step of 0.01 K.) The solution from applying equations (3), (6), and (7) to the set of generated fluxes is then  $T_X = 9186 \text{ K}$ ,  $t_X^2 = 0.043659$ —in very close accord with the Orion solution ( $T_X = 9185 \text{ K}$ ,  $t_X^2 = 0.043667$ ). The test case  $T_X$  is 337 K too low, and  $t_X^2$  is 0.01217 too large, compared to the true (analytical) values. We shall use these as our preferred correction necessary for the comparable Orion set.

This tailor-made test case may also be used to estimate the errors in our assessment of  $(N^+/O^+)_{\text{opt}}$  and  $(N^+/O^+)_{\text{uv}}$ . At  $N_e \sim 7000$ , all of the  $\epsilon$  values for the  $O^+$  lines are substantially different from their low-density limit values, as discussed earlier. The application of equations (16) and (17) to the “generated observed fluxes” yields  $(N^+/O^+)_{\text{opt}}$  and  $(N^+/O^+)_{\text{uv}}$  that are respectively a factor 1.031 too small and 1.037 too large compared to the original input ratio. These small corrections have not been applied in Figure 6. They would cause the right end of the curves for  $(N^+/O^+)_{\text{opt}}$  to rise and  $(N^+/O^+)_{\text{uv}}$  to drop by the same factors as above. While the small cumulative difference technically will cause the curves not to intersect, it is clear that the best inferred  $N^+/O^+$  is still  $\sim 0.14$ .

## REFERENCES

- Baldwin, J. A., Ferland, G. J., Martin, P. G., Corbin, M. R., Cota, S. A., Peterson, B. M., & Slettebak, A. 1991, *ApJ*, 374, 580  
 Balick, B., Gammon, R. H., & Hjellming, R. M. 1974, *PASP*, 86, 616  
 Bucseala, E. J., & Sharp, W. E. 1989, *J. Geophys. Res.*, 94, 12069  
 Calamai, A. G., & Johnson, C. E. 1991, *Phys. Rev. A*, 44, 218  
 Conti, P. S., Leitherer, C., & Vacca, W. D. 1996, *ApJ*, 461, L87  
 Davidson, K., Dufour, R. J., Walborn, N. R., & Gull, T. R. 1986, *ApJ*, 305, 867  
 DeRobertis, M. M., Dufour, R. J., & Hunt, R. W. 1987, *JRASC*, 81, 195  
 Fang, Z., & Kwong, V. H. S. 1997, *ApJ*, 474, 529  
 Froese-Fischer, C., & Saha, H. P. 1985, *Phys. Scr.*, 32, 181  
 Grevesse, N., & Noels, A. 1993, in *Origin and Evolution of the Elements*, ed. N. Prantzos, E. Vangioni-Flam, & M. Casse (Cambridge Univ. Press), 15  
 Harrington, J. P., Seaton, M. J., Adams, S., & Lutz, J. H. 1982, *MNRAS*, 199, 517  
*HST Data Handbook 1995, Version 2* (Baltimore: STScI)  
 Kingdon, J., & Ferland, G. J. 1995, *ApJ*, 450, 691  
 Lennon, D. J., & Burke, V. M. 1994, *A&AS*, 103, 273  
 Lester, D. F., Dinerstein, H. L., Werner, M. W., Watson, D. M., Genzel, R., & Storey, J. M. V. 1987, *ApJ*, 320, 573  
 Liu, X., Storey, P. J., Barlow, M. J., & Clegg, R. E. S. 1995, *MNRAS*, 272, 369  
 Maciejewski, W., Mathis, J. S., & Edgar, R. J. 1996, *ApJ*, 462, 347  
 Martin, P. G., et al. 1998, in preparation  
 Mathis, J. S. 1995, *Rev. Mexicana Astron. Astrofis. Conf. Ser.*, 3, 207  
 McLaughlin, B. M., & Bell, K. L. 1993, *ApJ*, 408, 753  
 Mendoza, C. 1983, in *IAU Symp. 103, Planetary Nebulae*, ed. D. R. Flower (Dordrecht: Reidel), 143  
 Meyer, D. M., Jura, M., Hawkins, I., & Cardelli, J. A. 1994, *ApJ*, 437, L59  
 Mihalszki, J. S., & Ferland, G. J. 1983, *PASP*, 95, 284  
 Nahar, S. N. 1996, *ApJS*, 106, 213  
 Nussbaumer, H., & Storey, P. 1983, *A&A*, 126, 75  
 ———. 1984, *A&AS*, 56, 293  
 O’Dell, C. R., Valk, J. H., Wen, Z., & Meyer, D. M. 1993, *ApJ*, 403, 678  
 Peimbert, M. 1967, *ApJ*, 150, 825  
 ———. 1993, *Rev. Mexicana Astron. Astrofis.* 27, 9  
 Peimbert, M., & Costero, R. 1969, *Bol. Obs. Tonantzintla Tacubaya*, 5, 229  
 Peimbert, M., Storey, P. J., & Torres-Peimbert, S. 1993, *ApJ*, 414, 626  
 Penston, M. V., et al. 1983, *MNRAS*, 202, 833  
 Péquignot, D., Petitjean, P., & Boisson, C. 1991, *A&A*, 251, 680  
 Petuchowski, S. J., & Bennett, C. L. 1995, *ApJ*, 438, 735  
 Pradhan, A. K. 1976, *MNRAS*, 177, 31  
 Rubin, R. H. 1969, *ApJ*, 155, 841  
 ———. 1985, *ApJS*, 57, 349  
 ———. 1986, *ApJ*, 309, 334  
 Rubin, R. H., et al. 1995, *STScI Symp., The Analysis of Emission Lines*, ed. R. E. Williams & M. Livio (Baltimore: STScI), 66  
 Rubin, R. H., et al. 1997, *ApJ*, 474, L131  
 Rubin, R. H., Simpson, J. P., Erickson, E. F., & Haas, M. R. 1988, *ApJ*, 327, 377  
 Rubin, R. H., Simpson, J. P., Haas, M. R., & Erickson, E. F. 1991a, *ApJ*, 374, 564  
 Rubin, R. H., Simpson, J. P., Haas, M. R., & Erickson, E. F. 1991b, *PASP*, 103, 834  
 Rubin, R. H., Simpson, J. P., Lord, S. D., Colgan, S. W. J., Erickson, E. F., & Haas, M. R. 1994, *ApJ*, 420, 772  
 Shaver, P. A., McGee, R. X., Newton, L. M., Danks, A. C., & Pottasch, S. R. 1983, *MNRAS*, 204, 53  
 Shaw, R. A., & Dufour, R. J. 1995, *PASP*, 107, 896  
 Simpson, J. P., Colgan, S. W. J., Rubin, R. H., Erickson, E. F., & Haas, M. R. 1995, *ApJ*, 444, 721  
 Soderblom, D. R., et al. 1995, *Instrument Handbook for the GHRS*, Vers. 6.0 (Baltimore: STScI)  
 Stafford, R. P., Bell, K. L., Hibbert, A., & Wijesundera, W. P. 1994, *MNRAS*, 268, 816  
 Stasinska, G., & Schaerer, D. 1997, *A&A*, 322, 615  
 Storey, P. J., & Hummer, D. G. 1995, *MNRAS*, 272, 41  
 Sun, Y., Sadeghpour, H. R., Kirby, K., Dalgarno, A., & Lafyatis, G. P. 1996, *Int. Rev. Phys. Chem.*, 15, 53  
 Vassiliadis, E., et al. 1996, *ApJS*, 105, 375  
 Vila-Costas, M. B., & Edmunds, M. G. 1993, *MNRAS*, 265, 199  
 Walter, D. K., & Dufour, R. J. 1998, in preparation  
 Walter, D. K., Dufour, R. J., & Hester, J. J. 1992, *ApJ*, 397, 196  
 Wheeler, J. C., Sneden, C., & Truran, J. W. 1989, *ARA&A*, 27, 279  
 Wiese, W. L., Fuhr, J. R., & Deters, T. M. 1996, *NIST Monograph 7, Atomic Transition Probabilities of Carbon, Nitrogen, and Oxygen*, A critical Data Compilation, *J. Phys. Chem. Ref. Data*  
 Williams, R. E., et al. 1985, *MNRAS*, 212, 753  
 Zuckerman, B. 1973, *ApJ*, 183, 863